CATHOLIC UNIVERSITY OF PERNAMBUCO
POSTGRADUATION PROGRAM IN CIVIL ENGINEERING

KLAYNE KATTILEY DOS SANTOS SILVA

ON THE USE OF EMBEDDED FIBER OPTIC SENSORS FOR MEASURE STRAINS IN CONCRETE

FRANCE
2021

KLAYNE KATTILEY DOS SANTOS SILVA

ON THE USE OF EMBEDDED FIBER OPTIC SENSORS FOR MEASURE STRAINS IN CONCRETE

Dissertation presented to the Catholic University of Pernambuco and Institut Catholique d'Arts et Metiers in partial fulfillment of the requirements for the degree of Master in Civil Engineering, in the area of Construction Materials.

Dissertação apresentada à Universidade Catolica de Pernambuco e Institut Catholique D'arts et Metiers como parte dos requisitos exigidos para a obtenção do título de Mestre em Engenharia Civil, na área de Materiais de Construção

Advisor: Prof, PhD Fernando Artur NOGUEIRA SILVA

Co-Advisors: Prof, PhD Mahfoud TAHLAITI and Prof, PhD Abdelhafid Khelidj

FRANCE

2021

S586o Silva, Klayne Kattiley dos Santos.
On the use of embedded fiber optic sensors for measure strains in concrete / Klayne Kattiley dos Santos, 2021.
90 f. : il.

Orientador: Fernando Artur Nogueira Silva.
Coorientadores: Mahfoud Tahlaiti, Abdelhafid Khelidj.
Dissertação (Mestrado) - Universidade Católica de Pernambuco. Programa de Pós-graduação em Engenharia Civil. Mestrado em Engenharia Civil, 2021.

1. Engenharia de estruturas. 2. Detectores. 3. Concreto armado. 4. Fibras ópticas. I. Título.

CDU 624.012.45

Pollyanna Alves - CRB-4/1002

Cataloging-in-Publication Data

Documentation and Information Division

DOS SANTOS SILVA, klayne kattiley

ON THE USE OF EMBEDDED FIBER OPTIC SENSORS FOR MEASURE STRAINS IN CONCRETE

KLAYNE KATTILEY DOS SANTOS SILVA, Recife, 2021

Master Thesis – Civil Engineering – Catholic University of Pernambuco, 2020.
Advisor: PhD Fernando Artur Nogueira Silva. Co-Advisor: PhD Mahfoud Tahlaiti

1. Fiber optic sensors (FOS) 2. Concrete 3. Internal swelling reactions (ISR) 4. Shrinkage
5. Fiber Bragg Grating (FBG)

BIBLIOGRAPHIC REFERENCE

DOS SANTOS SILVA, klayne kattiley. **ON THE USE OF EMBEDDED FIBER OPTIC SENSORS FOR MEASURE STRAINS IN CONCRETE**, 2021. 90 P. Master Thesis - Civil Engineering – Catholic University of Pernambuco, Recife, Brazil.

UNIVERSIDADE CATÓLICA DE PERNAMBUCO
PRÓ-REITORIA DE PESQUISA, PÓS-GRADUAÇÃO E INOVAÇÃO
COORDENAÇÃO DA PÓS-GRADUAÇÃO STRICTO SENSU
PROGRAMA DE PÓS-GRADUAÇÃO EM ENGENHARIA CIVIL - MESTRADO

CATÓLICA

ATA DE DEFESA DA DISSERTAÇÃO DE MESTRADO DA ALUNA

KLAYNE KATTILEY DOS SANTOS SILVA

Aos onze dias do mês de fevereiro do ano de dois mil e vinte e um, realizou-se, às treze horas e trinta minutos, em Recife-PE, por *Google Meet*, remotamente e mediada pelas tecnologias digitais da informação e comunicação, a sessão pública de Defesa da Dissertação **"ON THE USE OF EMBEDDED FIBER OPTIC SENSORS FOR MEASURE STRAINS IN CONCRETE",** apresentada e defendida pela mestranda KLAYNE KATTILEY DOS SANTOS SILVA, Bacharela em Engenharia Civil pela Universidade Católica de Pernambuco, e que concluiu os créditos exigidos para obtenção do título de "Mestra em Engenharia Civil", segundo encaminhamento do Prof. Dr. Joaquim Teodoro Romão de Oliveira, Coordenador do Programa de Pós-graduação em Engenharia Civil - Mestrado desta Universidade, e documentação constante nos arquivos da Secretaria de Registros Acadêmicos, desta Pró-reitoria. Os trabalhos foram instalados e coordenados pelo Prof. Dr. Fernando Artur Nogueira Silva, Presidente da Banca Examinadora, constituída pelos Professores Doutores: Joaquim Teodoro Romão de Oliveira, da Universidade Católica de Pernambuco, Abdelhafid Khelidj, da Université de Nantes, Antônio Augusto Costa de Azevedo, do Instituto Federal de Pernambuco e Fernando Artur Nogueira Silva, da Universidade Católica de Pernambuco, Orientador da mestranda, presentes, remotamente, por videoconferência, em conformidade com a Portaria nº 36 da Coordenação de Aperfeiçoamento de Pessoal de Nível Superior - CAPES - de 19 de março de 2020. A aluna teve como Coorientador o Prof. Dr. Mahfoud Tahlaiti. O Prof. Dr. Fernando Artur Nogueira Silva, como Presidente da Banca Examinadora, solicitou à mestranda que apresentasse sua Dissertação em ambiente digital. Em seguida, a Banca tendo decidido aceitar a Dissertação passou à arguição pública da mestranda. Encerrados os trabalhos de arguição, os examinadores deram o parecer final sobre a Dissertação, tendo sido a candidata **APROVADA**, por todos os membros da Banca Examinadora e para constar, foi lavrada a presente Ata, que vai assinada, digitalmente, pelos membros da Banca Examinadora. Recife, 11 de fevereiro de 2021.

Prof. Dr. Joaquim Teodoro Romão de Oliveira

Prof. Dr. Abdelhafid Khelidj

Prof. Dr. Antônio Augusto Costa de Azevedo

Prof. Dr. Mahfoud Tahlaiti

Prof. Dr. Fernando Artur Nogueira Silva
President of the Examining Committee

ICMN
(5280.2-0)

This work is dedicated to my professors, for inspiring me every day and for making me dream of being like them.

ACKNOWLEDGEMENT

First of all, I would like to thank God and my family, for being the basis on which my life is sustained.

Thanks to the CAPES for financing this project and the institutions responsible for this project, both UNICAP and ICAM-Nantes, for all the support they have given me.

I am very grateful to my advisors Dr. Mahfoud Tahlaiti, Prof. Dr. Fernando Arthur and Prof. Dr. Abdelhafid Khelidj for the guidance and careful analysis of what I did during this extremely important period in my life and in the life of my family.

Thanks to Prof. Veronique Lefeuvre Arias for teaching French, in which I was able to evolve a lot because I had your support and good classes.

I am especially grateful to my other professors from Brazil who supported me during this period, Prof. Dr. Joaquim Oliveira, Prof. Dr. Antonio Augusto, Profa. Dr. Maria da Graça, Prof. Antonio Flavio, Prof. Pedro Eugenio, Prof. Sergio Dias and many others for making everything possible, for believing in me, giving me the financial and moral support I needed to carry out this work.

Thanks to friends and teachers at Santa Ines school, to Dr. Jose Alexandre Saraiva and so many friends from my city, who believed that I would be able to win this stage more.

To the friends that I made in Nantes, Rodrigo Roma, Ícaro Ladeira, Marc Congolo, Ye Pyae Sone Oo, Chisom Bernard, Celia Mir Alvarez, Fatima Ezzahra Kab, Annie and so many others for sharing laughter, love, good food and incredible moments by my side .

Anyway, all my love to my family, friends and professors, for everything they did for me.

ABSTRACT

Concrete is one of the main materials used worldwide and the quest to improve the quality and durability of concrete structures is constant. Several factors can contribute to the decrease of the durability of the material, deformations caused by phenomena such as Shrinkage and internal swelling reactions occur for different causes and generally at different ages, but they can directly interfere in decreasing the useful life of the structures.There are several test methods used to describe the behavior of structures against retraction or affected by internal swelling reactions (ISR), but most of them require complex and destructive procedures for material analysis. Over time, new technologies have been the subject of study for monitoring structures over time, including fiber optic sensors, so fiber optic sensors have been increasingly applied to the study of concrete elements and engineering in general. There are several types and designs of sensors, but not all are suitable for use in concrete structures. This work aims to evaluate whether this technology is effective as an alternative for monitoring concrete. The analysis of deformations from Shrinkage and internal swelling reactions in concrete elements was done using a bare-type, small-diameter FBG (Fiber Bragg Grating) sensor.

Keywords: Fiber optic sensors (FOS), Concrete, Internal swelling reactions (ISR), Shrinkage, Fiber Bragg Grating (FBG)

LIST OF FIGURES

LIST OF TABLES

LIST OF ABBREVIATIONS AND ACRONYMS

AAR: Alkali-Aggregate Reaction

ACR: Alkali-Carbonate Reaction

ASR: Alkali-Silica Reaction

ASSR: Alkali-Silicate Reaction

ASTM: American Society for Testing and Materials

DEF: Delayed Ettringite Formation

EFOS: Extrinsic Fiber Optic Sensor

ESA: External Sulfate Attack

FBG: Fiber Bragg Grating

FOS: Fiber Optic Sensor

FP: Fabry-Perot

IFOS: Intrisic Fiber Optic Sensor

ISA: Internal Sulfate Attack

ISR: Internal Swelling Reaction

RILEM - Reunion Internationale Des Laboratoires D'essais Et De Recherche Sur Les Materiaux Et Les Constructions

SHM: Structural Health Monitoring

SUMMARY

1 INTRODUCTION

Concrete is the most versatile and widely used building material in many types of structures around the world. Since the manufacture of concrete until the end of useful life, the material suffers deformations, these deformations or volumetric variations can be caused by external factors (environmental conditions, applied loads, etc.) or by internal factors (chemical reactions, pathologies, etc.) Deformations in concrete structural elements, depending on how and when they occur, directly contribute to the occurrence of cracks, which in turn interfere with the durability of the material.The presence of cracks in the concrete, which are the result of deformations in the material, can indicate the deterioration of the structures, so it is necessary to implement systems capable of monitoring the structural conditions over time.

It is know that initially the concrete is presented as a fluid, this phase of the material is called fresh state, which goes from the first interaction between water and cement (chemical process), until the beginning of the hardening of the material, at this moment the so-called hardened state of the material begins. This transition from one state to the other is very important and it is in this phase that shrinkage occurs, which is basically the reduction of the volume of the material due to water loss. This change in volume may cause cracks to appear in the material, due to which various structural problems may occur. (ŠAHINAGIĆ-ISOVIĆ et al. 2012)

Although, at the beginning, the cracks caused by shrinkage are combated with the proper curing of the material, throughout the useful life of the concrete, the material may present various types of pathologies. According Sims and Poole (2017) these pathologies can be the result of a series of factors ranging from the imprudent selection of the materials used to manufacture the material to execution failures, inadequate sizing and overloading of concrete elements.

Internal swelling reactions (ISR) are examples of pathologies that can occur throughout the useful life of concrete. These reactions are related to chemical interactions that have physical implications for concrete structures. These expansion mechanisms can be divided into two main groups: Alkali-aggregate reaction (AAR) and delayed ettringite formation (DEF). The origins of these reactions are different, but both lead to the expansion of the affected concrete elements, especially in the presence of humidity. (NOEL, SANCHEZ and TAWIL, 2017)

On a macroscopic scale, both AAR and DEF cause very similar cracks in the concrete structural elements, but originally the AAR phenomenon occurs due to the presence of reactive aggregates in the mixture, high concentration of alkalis in the cement used and the presence of humidity, while DEF occurs due to the natural process of cement hydration, where ettringite develops late. The factors presented

above may cause the concrete element to require costly repairs or replacement, so it is necessary to detect and monitor deformations, however, the existing methods used to diagnose and describe the behavior of structures affected by pathologies, especially in the case of internal swelling reactions, are destructive methods, which require the removal of parts of the structure for a more detailed analysis.

Over time, new technologies have been studied to monitor structures, including fiber optic sensors. Optical fiber detection systems have been successfully developed for many engineering applications and tend to be an important resource for monitoring concrete structures in a non-destructive way.

According to Mendez *et al.* (1990) the development of fiber optic technologies for the civil engineering sector is attractive because, in addition to the possibility of assessing the mechanical conditions of the structure, it also involves the social character that the buildings represent.

Optical fiber technology is well dominated today, after decades of development. Although there are many types, almost all optical fibers are based on the same principle: the total reflection of a ray of light within a waveguide. Optical fibers, therefore, use a non-electric light signal to transmit information, which offers significant advantages such as sensitivity to electromagnetic disturbances and the high speed of signal propagation.

Due to their precision and small size, fiber optic sensors (FOS) can provide information that is not reachable with existing techniques and, therefore, enable the acquisition of new information useful for the evaluation of structural conditions, such as information on deformations, temperature and other related aspects for concrete. (LEUNG, 2001)

In general, fiber optic sensors are capable of providing "real-time" information on the state of a specific structure or concrete member by means of a built-in damage detection and assessment system based on a fiber optic grid embedded in the structure at the time of construction. It is an important resource that can bring great benefits to the construction industry, but with the multitude of existing fiber designs, it is necessary to choose the most appropriate type, bearing in mind that the objective is to ensure the effective monitoring of concrete structures over a long period of time.

In order to find new structural monitoring resources, less invasive and more accurate, this work aims to study the viability of fiber optics sensor type FBG, without coating, to obtain information about the deformations that can occur due to shrinkage and internal swelling reactions.

1.1 OBJECTIVES

1.1.1 General Objective

The aim of this research is to investigate the potential of using Fiber Bragg grating sensor to measure the strain in concrete elements by Shrinkage and affected by internal swelling reactions.

1.1.2 Specific Objectives

- Make concrete prisms to analyze with optical fiber the deformations caused in the concrete by Shrinkage;
- Subject some prisms to extreme conditions capable of accelerating ISR's;
- Obtain levels of expansion through the use of fiber optics;
- Analyze whether the design of the optical fiber used is suitable for this type of concrete study;

2 LITERATURE REVIEW

2.1 SHRINKAGE STRAIN OF CONCRETE

One of the phenomena that can cause volumetric changes in concrete structural elements is called is called shrinkage.This phenomenon causes the decrease in concrete volume due to moisture loss and occurs in cement and mortar matrices. The shrinkage is directly related to the hydration reactions between cement and water and the progressive hardening of the material. (BAZANT and WITTMANN, 1982)

According to Sellier et al. (2016), this phenomenon is complex and, depending on how and when it occurs, can cause cracks that are responsible for serious durability problems that are detrimental to the performance and useful life of concrete structures.

For a better understanding of the phenomenon, it is important to know that there are three main types of shrinkage, they are: plastic shrinkage, autogenous shrinkage and drying shrinkage.

2.1.1 Plastic Shrinkage

The plastic shrinkage in a concrete occurs in the plastic phase of the material, as the name suggests. The loss of water by evaporation from its surface, after the release of the material into the forms and before the hardening of the concrete can lead to cracks by plastic shrinkage if the rate of moisture loss by evaporation is higher than that of the water that rises to the surface of the concrete after the thickening of the material. (DHIR et al., 2019)

On the surface, plastic shrinkage occurs when the rate of evaporation exceeds the rate of bleeding and can be noticed on the surface of the bridge slabs and trays in the form of cracks, which can occur before or during finishing operations. Plastic shrinkage cracks initially start as shallow cracks, but can develop into deeper cracks that can cause maintenance and durability problems. Cracking by plastic shrinkage is inevitable if there is sufficient tensile strength to overcome the tensile stress caused by the restriction influence of the concrete below the drying surface. (ALLENA, 2011)

According Brooks (2007) the prevention of cracks by plastic shrinkage is possible by covering the concrete surface as early as possible and protecting it from the effects of drying winds. The spraying of resin-based curing compounds (except in the form of an emulsion) cannot be done effectively until the free water has evaporated.

Therefore, it is difficult to ensure that the compound is applied before the plastic shrinkage cracks start to form. Covering with polyethylene sheet is the most effective solution. The Figure 1 presents the mechanism of plastic shkrinkage

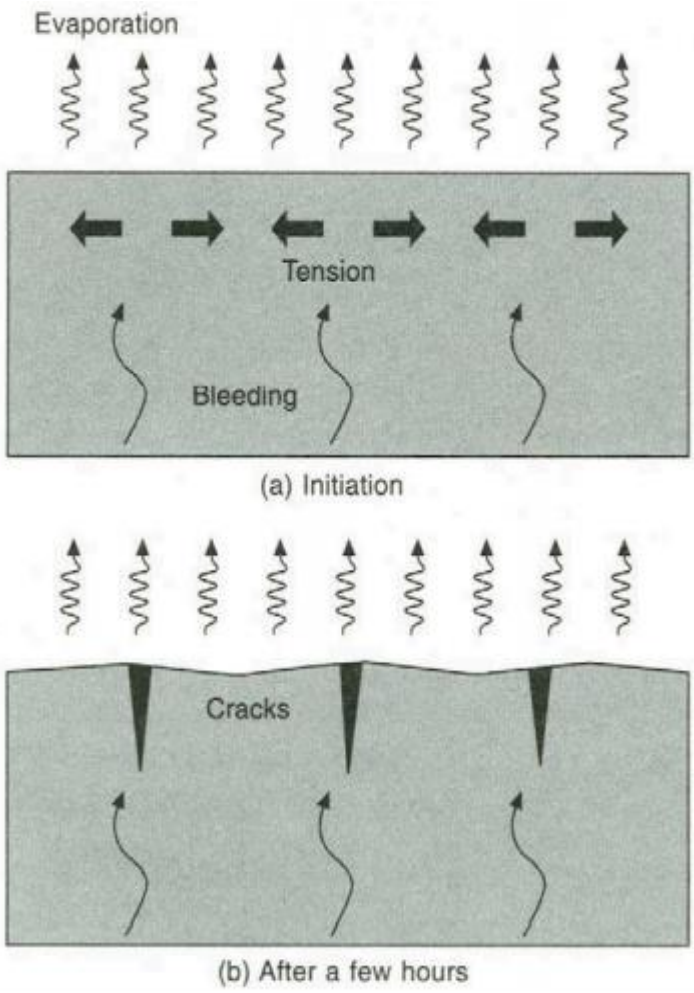

Figure 1: The mechanism of plastic shkrinkage (Day & Clark, 2003)

2.1.2 Drying Shrinkage

Drying shrinkage can easily be defined as deformation due to water loss from the concrete in the hardened state. In this case, the aggregated particles settle on the fresh concrete and the water moves to the concrete surface like bleeding water. Bleeding water evaporates from the concrete surface due to environmental factors, and the concrete surface is subjected to drying while the water is removed from inside the concrete. (ALLENA, 2011)

According to Bazant & Jirásek (2018) in conventional concretes, most of the shrinkage represents drying shrinkage, which is mainly caused by the increase in the capillary tension of the pore water and the solid surface tension of the pore

walls, as well as by the narrowing of multimolecular hindered adsorbed water layers in cement gel micropores. The magnitude of the contraction strain ε_{sh} is an increasing function of time (Figure 2) that approaches a finite limit at a gradually decreasing rate.

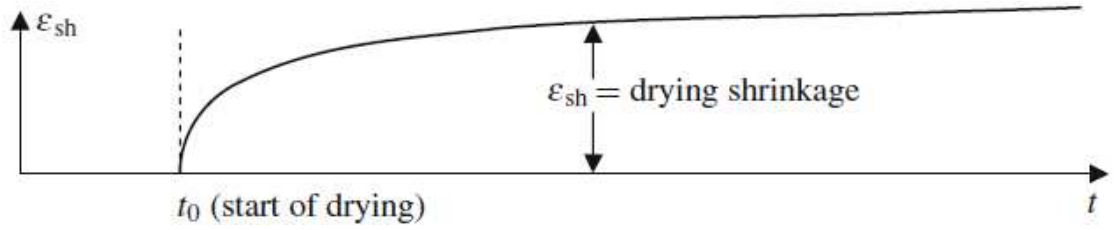

Figure 2: Shkrinkage Time-Dependent Deformation (Bazant & Jirásek, 2018)

According Mehta & Monteiro (2014) Drying shrinkage can be classified as reversible or irreversible (Figure 3). Reversible drying shrinkage refers to the diffusion of moisture, the part of the total shrinkage of which can be reproduced by wetting-drying cycles. On the irreversible side, it is no longer possible for the structure to recover from deformation due to shrinkage, even after a long period of storage in water.

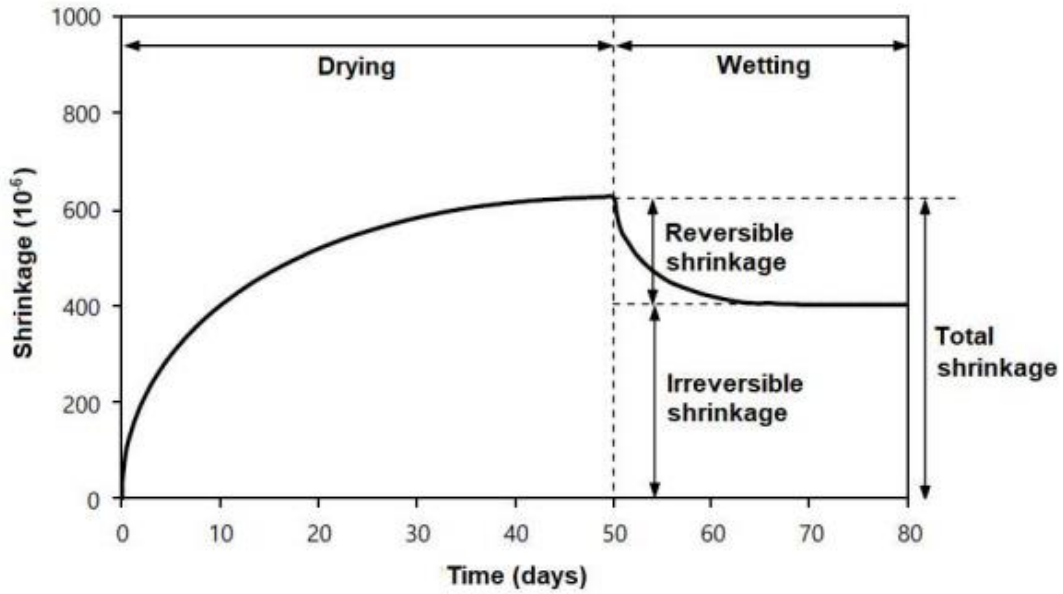

Figure 3: Drying shrinkage classification (Mehta & Monteiro, 2014)

The causes of shrinkage cracks are numerous, the main ones being inefficient or insufficient joints, inadequate reinforcement, deficient curing and very high water content in the concrete mixture. The form of restriction can be internal or external. Figure 4 shows an example of an external constraint on an unreinforced concrete

slab drying from the surface. If, after being relieved by creep, the induced tensile stress exceeds the resistance, the result would be a single crack in the slab. (BROOKS, 2007)

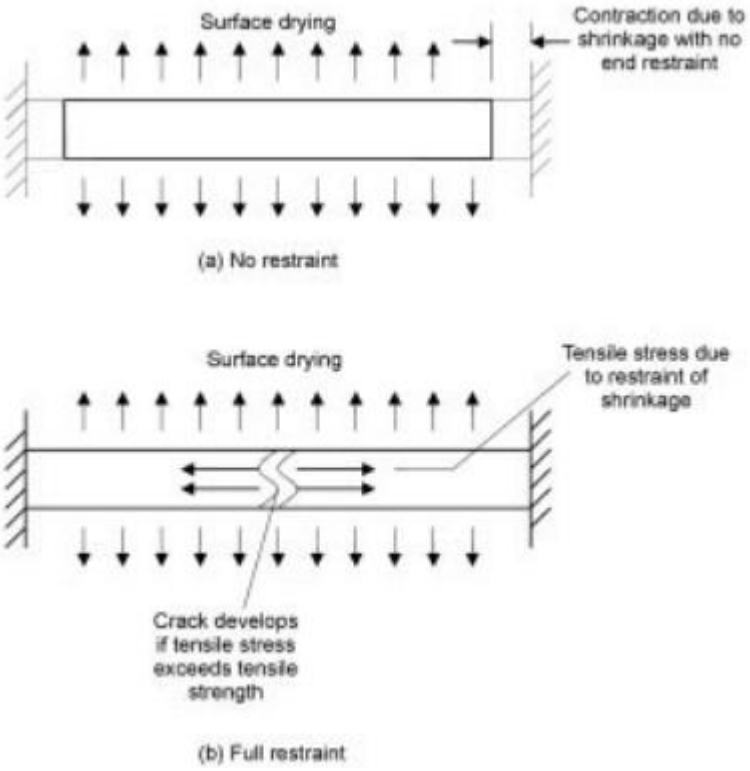

Figure 4: Example of full restraint of drying shrinkage in a concrete slab (Brooks, 2007)

ASTM C 157 / C 157M, "Standard Test Method for Length Change of Hardened Hydraulic-Cement Mortar and Concrete" (2008) shows how to calculate shrinkage by drying on concrete elements. Usually the value is expressed as a percentage or in millionths ($x10^{-6}$). Physically, concrete that experiences a drying shrinkage of about 0.05 percent (500 millionths or 500 x 10-6) will shrink by approximately 0.6 in. per 100 feet (50 mm for every 100 m).

2.1.3 Autogenous Shrinkage

Autogenous shrinkage is more related to the chemical process that cement-based materials undergo during hydration. That is, autogenous shrinkage refers to chemical shrinkage. When external water is not available for hydrating the cement, water from the internal pore is used for the hydration reaction. This phenomenon of water withdrawal from capillary pores due to hydration is known as self-desiccation. (KOVLER & ZHUTOVSKY, 2006)

According to Neville (2004), Autogenous shrinkage is predominant in concrete with a low water-cement ratio, that is, autogenous shrinkage occurs in many different types of concrete, but it is more expressive in high-strength concrete and concrete mass, in these conditions the autogenous shrinkage is high (700 microstrain). The Figure 5 shows a comparison between drying shrinkage and autogenous shrinkage for conventional concrete and high performance concrete.

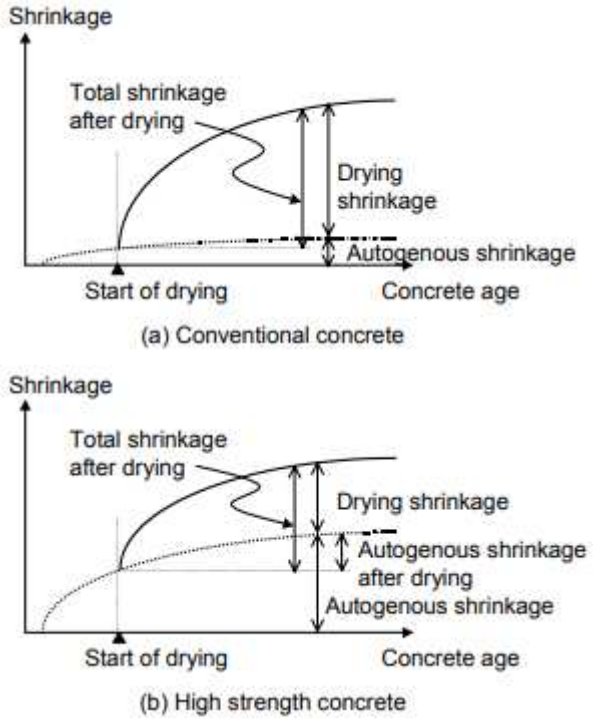

Figure 5: Shrinkage strain in normal concrete (a) and high-strength (b) (Sakata & Shimomura 2004)

2.1.4 Factors Affecting Shrinkage of Concrete

Several authors (MEHTA & MONTEIRO, 2014; BROOKS, 1992; KHAYAT, 2009; NEVILLE, 2004; BAZANT 2000) present the main factors that influence the occurrence of concrete shrinkage, for this reason, they will only be briefly discussed in this section.

The main influencing factors for the occurrence of retraction are:

a) Environmental conditions (relative humidity and temperature);
b) Aggregate concentration;
c) Water to cement ratio (w/c);
d) Addition of admixtures;
e) Curing conditions;
f) Element Geometry;
g) Age of the Concrete;
h) Intensity and Age of the Loading.

As already presented, one of the main consequences of the retraction is the cracks that can appear in the concrete, Figure 6 presents a scheme of the characteristics of the types of cracks that can occur due to the different types of retraction.

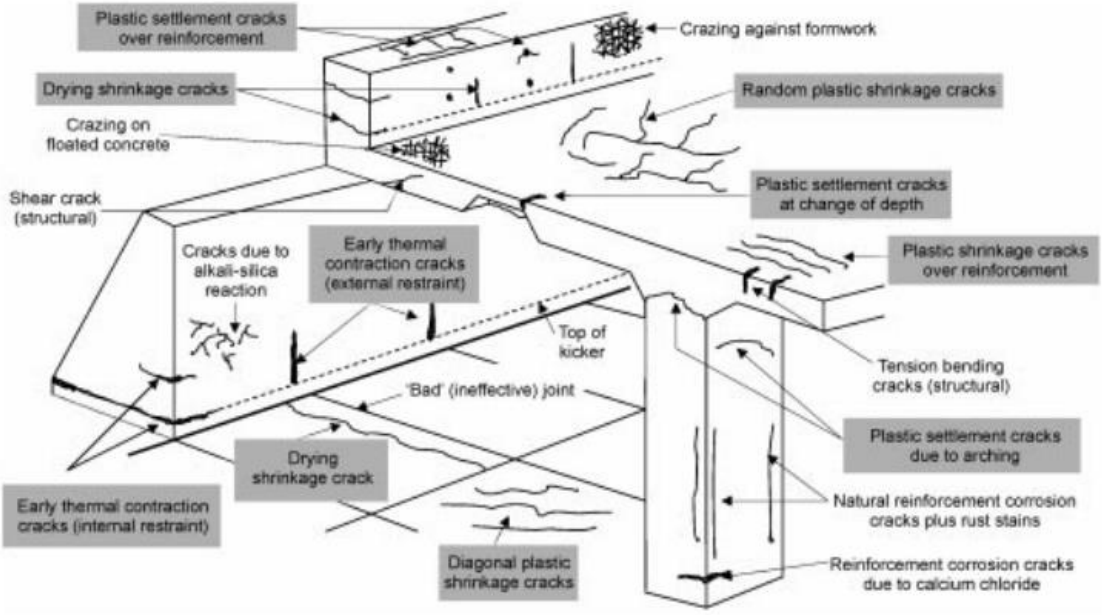

Figure 6: Examples of cracks in a schematic concrete structure (Brooks, 2007)

2.2 INTERNAL SWEELING REACTIONS (ISR)

Other phenomena capable of causing concrete volumetric changes are the so-called internal swelling reactions. Unlike the shrinkage presented above, these reactions cause expansion in the concrete and can be divided mainly between alkali-aggregate reaction (AAR) and delayed ettringite formation (DEF).

According Martin *et al.* (2012) these reactions that cause expansion of the affected concrete, which will be described in detail below, generally lead to cracking and a decrease in its mechanical properties of the material. As a consequence, these pathologies raise serious problems in terms of maintenance and structural integrity.

2.2.1 Alkali-Aggregate Reaction (AAR)

AAR's first records were made in the state of California in the 1930s by Thomas Stanton of the California State Highways Division. The identification of the problem was reported by the same in 1940 (Stanton 1940). Stanton identified the expansion of the mortar bars

and observed that this expansion was influenced by the alkaline content of the cement, the type and amount of reactive silica present in the aggregate, the presence of moisture and also the temperature. Following Stanton's discovery, AAR was diagnosed as the cause of cracking in several dams operated by the US Bureau of Reclamation, such as Parker Dam in Arizona (Meissner 1941), and in the 1940s several entities began studies of AAR in the USA. (Army Corps of Engineers, Department of Public Roads, Portland Cement Association) and several other countries. (THOMAS, FOURNIER and FOLLIARD, 2013).

The reaction between the aggregate and the alkalis has been called the "alkalis-aggregate reaction". Stanton's work changed the earlier view that the aggregate would be an inert filler, as it was realized that some aggregates were not suitable for use in concrete without taking special precautionary measures. In addition, Stanton's discovery that cement alkalis can influence the durability of concrete has raised some concerns among cement manufacturers. (SIMS and POOLE, 2017)

It is estimated that AAR is currently found in more than fifty countries, and since its discovery there are several scientific and technological advances in the prevention and diagnosis of this type of reaction. (FOURNIER and BÉRUBÉ, 2000)

2.2.1.1 Types OF AAR

a) Alkali-silica reaction (ASR):

AAR in the most common concrete is the alkali-silica reaction. It is a chemical reaction that occurs between amorphous silica present in reactive ions and hydroxyl in porous solution aggregates. ASR is a complex reaction and, for concrete to occur, three conditions must be met: the presence of reactive aggregate, a high level of alkalis, cement component and sufficient moisture, around 80% in the concrete pores. Without one of these conditions, ASR will not occur. (PAN *et al.*, 2012)

In the Fig. 7 it is possible to observe in a simplified way how the destructive process of ASR occurs in the concrete.

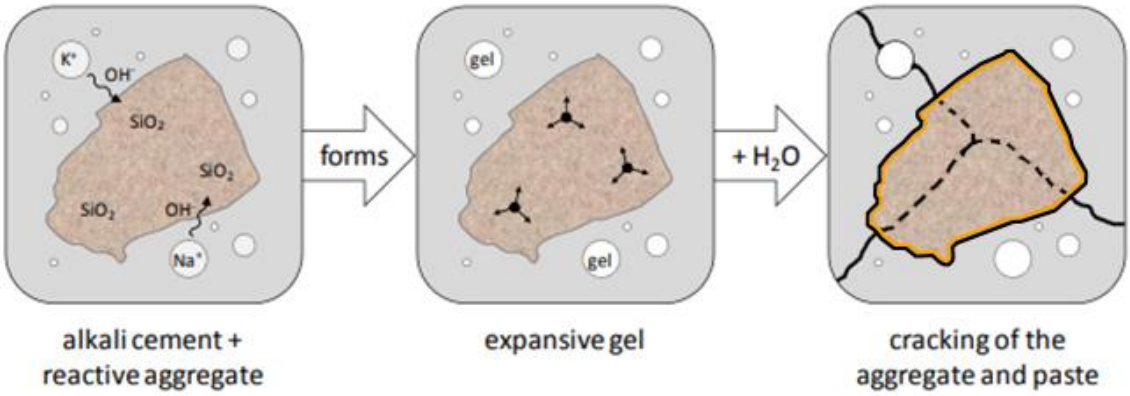

Figure 7: Alkali-Silica Reaction (Deschenes, 2009) adaptated

When present in the concrete, the reactive aggregates interact with the fluids present in the strongly alkaline pores (pH> 12) of the cement paste, this interaction causes depolymerization of the silica structure. The reaction products (gel formation) change in volume and can expand until the tensile strength of the concrete is overcome, causing the material to present a cracking frame. The speed of the reaction and the consequent damage to concrete depends of the characteristics of the aggregate and the cement paste. (PIGNATELLI, 2012)

b) Alkali-silicate reaction (ASSR):

The alkali silicate reaction is slower than ASR because the minerals that contribute to this reaction are in the crystalline reticulum. This type of reaction occurs among the alkalis found in cement and silicate found in feldspars in some sedimentary, metamorphic and magmatic rocks. (KIHARA, 1986)

According to Sanchez (2008), the gel formed by this reaction generates a very low adhesion between the aggregate and the concrete matrix. This gel may expand in the presence of water, causing cracking, which is a common feature of R.

In all alkali-silicate reaction cases, water inlet and outlet are essential for the expansion mechanism to occur, as well as the rock structure has a considerable influence on the proportion and degree of expansion, as the isolated minerals are expansive components. (GILLOTT, 1986)

c) Alkali-carbonate reaction (ACR):

In ACR, dolomite (calcium magnesium carbonate) ($CaMg(CO_3)_2$) reacts with sodium and potassium dissolved in the alkaline pore solution. The attack of alkalis on carbonate rocks is called decolomitization. After dedolomitization occurs, alkaline carbonate (sodium carbonate) reacts with the cement hydration products within the cement paste to form alkalis again, which will continue the dedolomitization reaction. This cycle will occur until the total consumption of dolomite or until the alkali concentration has been reduced by side reactions. (LEEMANN *et al*., 2016)

According to Swamy (1992) this process of crystal dedolomitization allows moisture to be absorbed and the expansion caused by this absorption is irreversible and causes the expansion and cracking of concrete.

According to Fournier and Bérubé (2000), this type of reaction is rare and was first identified in the 1950s in Canada, but there are not many records of this reaction in other parts of the world.

2.2.1.2 ASR Mechanism and Stages

The main reaction of the alkali silica reaction is that between the silica present in the aggregates and the hydroxide ions (OH^-) present in the pore water of a concrete. In this phase, the hydroxide ions attack the silica surface. If the silica has a stable and well crystallized network, there is a lesser chance of the attack occurring, considering that the vulnerable places will only be on the external surface of the aggregate (Fig 8a), however if the silica has an irregular formation and poorly crystallized, there will be many vulnerable locations in the aggregate structure, leading to the disintegration of the silicate network (Fig 8b). (FERRARIS, 1995)

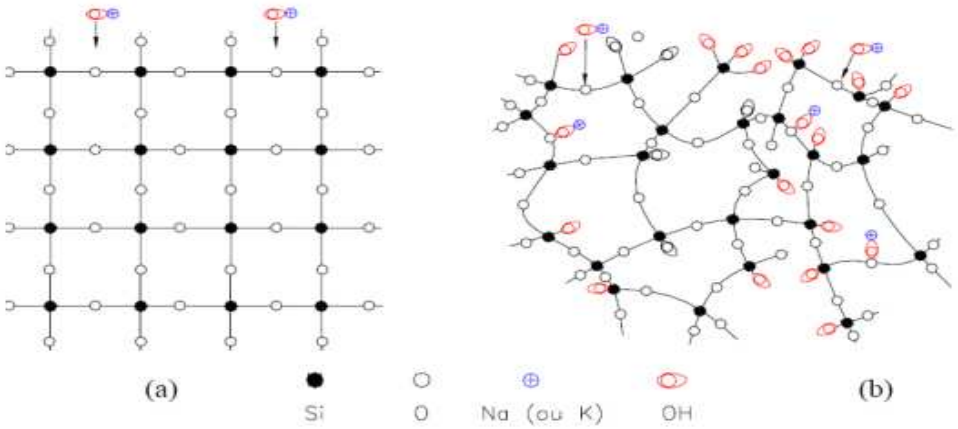

Figure 8: Schematic representation of the attack of alkaline solutions on sílica a) Well crystallized silica b) Poorly crystallized silica (Ferraris, 1995 *adapted by* Almeida, 2015)

This first process can be described through eq. 1, where R + represents the alkali metal ions (Li +, Na +, K +). Where the alkali metal ions (Li+, Na+, K+) are presented by R^+.

$$\equiv Si\text{-}O\text{-}Si \equiv + OH^- + R^+ \rightarrow \equiv Si\text{-}O\text{-}R + H\text{-}O\text{-}Si \equiv \quad (1)$$

According SAHA *et al*. (2018), the next process occurs when silicic acid reacts with the hydroxyl ions (OH-) and metal alkali that forms alkali silicate hydrate, in this process water is released, as shown in eq. 2.

$$\equiv Si\text{-}O\text{-}H + OH^- + R^+ \rightarrow \equiv Si\text{-}O\text{-}R + H_2O \quad (2)$$

In essence, this reaction is the same that occurs when the hydroxylated surface silica mentioned above is attacked by hydroxyl, except that it would precede the reaction given previously in such cases. (PETERSON *et al.* 2000)

Finally the formation of the gel occurs. The last process can be described for the eq. 3.

$$\equiv Si\text{-}O\text{-}R + nH2O \rightarrow \equiv Si\text{-}O^{-}\text{-}(H2O)_n + R^{+} \quad (3)$$

According Chatterji (1989) calcium ions ($Ca2^{+}$) play an important role in the process of forming the expansive gel present in the alkali-silica reaction. The diffusion of silica to other locations depends on the concentration of $Ca2^{+}$ locally. If the $Ca2^{+}$ concentration is low, the tendency for silica to diffuse is increased, implying that the reaction requires the presence of calcium ions. In addition the calcium is a very important role in determining where exactly the damaging gel will form. The source of calcium in concrete is the Portlandite crystals, Ca (OH) 2, which is a vast resource.

The reaction between the amorphous silica present in some types of aggregate and the hydroxide ions (OH^{-}) present in the porous solution results in the formation of a gel. (PETERSON, 2000)

The formation of the gel itself does not cause damage to the concrete, however this gel has the ability to expand in the presence of water. This expansion can cause cracks in the concrete structures due to the fact that the tensile strength supported by the material is exceeded by the gel. (FERRARIS, 1995)

According to Léger *et al.* (1996) evolution of the concrete expansion due to AAR over time, can be described, basically, in three main stages (Fig. 9).

a) The first moment deals with an initiation phase where the concrete mass becomes saturated by silico-alkaline gel, a by-product of AAR, which absorbs moisture and then expands. In this phase there is no significant expansion, as the pores of the concrete are not fully filled;

b) The second stage is the development phase. At this stage, the gel has already filled all the pores of the concrete and continues to absorb water, causing the expansion of the concrete to begin to occur;

c) Finally, the third stage is when the reactive material runs out, so that the gel formation stops and the expansion process stops.

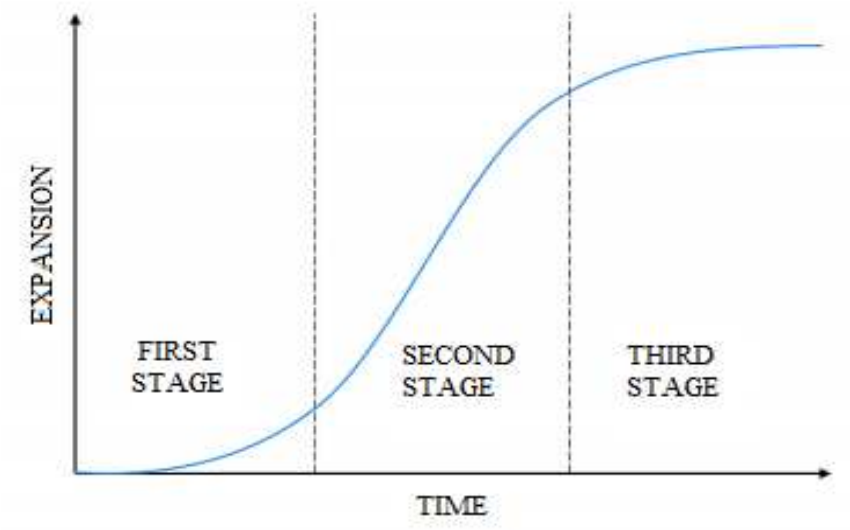

Figure 9: Stages of alkali-aggregate reaction
(Posterlli, 2017) Adapted

Saouma *et al.* (2015) presents a different approach to the reaction stages, this time from a petrographic point of view. For this author, the evolution of the reaction occurs in four different stages: nucleation, development of the raction, accelarating of the reaction and deterioration, and finally severe deterioration. The first three stages can be observed in detail in Fig. 10. The petrographic interpretation of the evolution of AAR can be observed in Fig. 11.

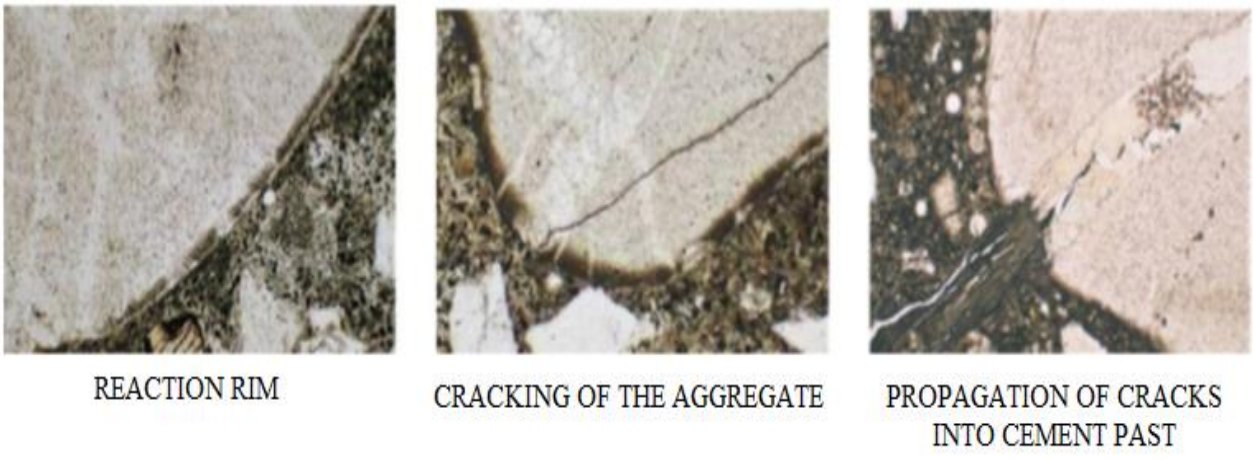

Figure 10: Crack nucleation inside aggregate followed by propagation inside the cement past.
(Katayama, 2012)

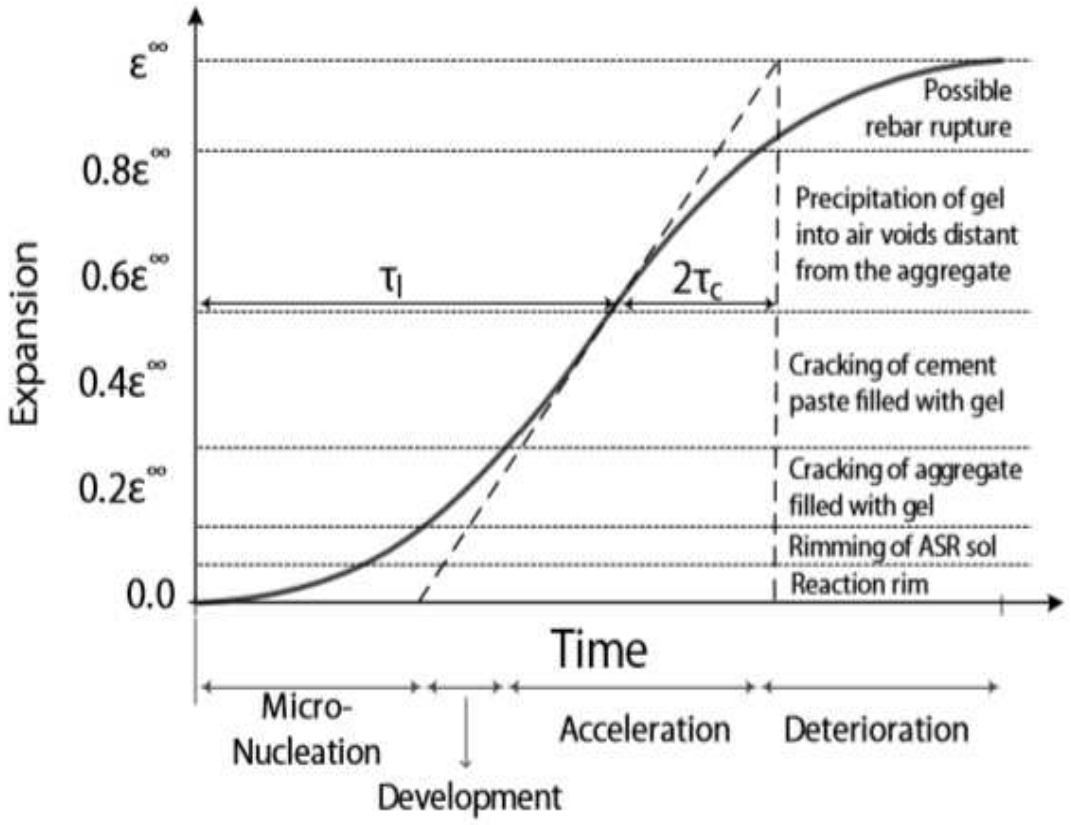

Figure 11: Petrographic interpretation of the evolution of AAR (Saouma, *et al.* 2015)

2.2.2 Delayed Ettringite Formation (DEF)

Sulphate attack represents a major risk for concrete structures. According to Devit (2001), attacks by sulfates were first reported in 1887 by Candlot in Paris, fortifications built on plaster floors.

According to Godart (2017) the first reported cases of DEF occurred in some precast concrete elements subjected to heat treatment inadequate to the concrete composition and the environment. The main reported cases of DEF worldwide include railway sleepers and components with large volumes of solid concrete. Most of the reported cases also include bridges. The parts damaged by DEF were mainly solid structural elements (pillars, beams or pillars, etc.) in contact with water or subject to high humidity. The sulphate activity that occurs when concrete undergoes a thermal process in the early ages is known in several countries and has been the subject of several studies worldwide.

Although AAR and DEF have similar effects and can appear in the structure in a combined way, these types of expansive reactions have completely different origins.

The formation of etringite occurs naturally in the cement hydration process, when the tricalcium aluminate (C_3A) reacts with gypsum and forms the primary ettringite. (Eq.4) when all the gypsum is consumed, the etringite can react even more with the remaining C_3A and form monosulfate in the first days. (Eq.5) Entringite can re-form later, after months or years, as long as there is a new source if sulfate is present in the solution of the cement paste pores, then it is when the so-called “delayed ettingite formation” occurs, therefore DEF, is associated with a damaging sulphate attack. (YU, et al. 2016)

$$C_3A + 3CSH_2 + 26\ H \rightarrow C_6\ AS_3\ H_{32} \quad (4)$$

$$2C_3A + C_6\ AS_3\ H_{32} + 4\ H \rightarrow 3C_4\ ASH_{12} \quad (5)$$

According Collepardi (2003) the attack by sulfate can occur from two different sources, internal and external. External sulfate attack (ESA) occurs when environmental sulfate (from water or soil) penetrates concrete structures. The internal sulfate attack (ISA) occurs in a sulfate-free environment when the sulfate source is inside the concrete and comes from cement with a high sulfate content or aggregate contaminated with plaster. Both cases must be taken into account in the study of structures that present the formation of DEF. More objectively, the attack by external sulfate occurs when there is the presence of moisture (intermittent or constant), the concrete is very permeable and the environment is rich in sulfate. The attack by internal sulfate is related to the thermal decomposition of primary etringite and late release of sulfate.

The chemical reactions that lead to DEF occur among several ionic species available in the pore solutions of concrete when the preliminary etringite was inhibited by high temperature (above 60-70 °C). This temperature may be due to steam curing processes or the cement hydration process itself, which is an exothermic reaction. (BOUZABATA *et al*., 2012)

Other authors such as collepardi (2003) and Karthik et al. (2016) state that this type of reaction occurs at temperatures above 70 ° C (158 ° F) as indicated in Fig 12.

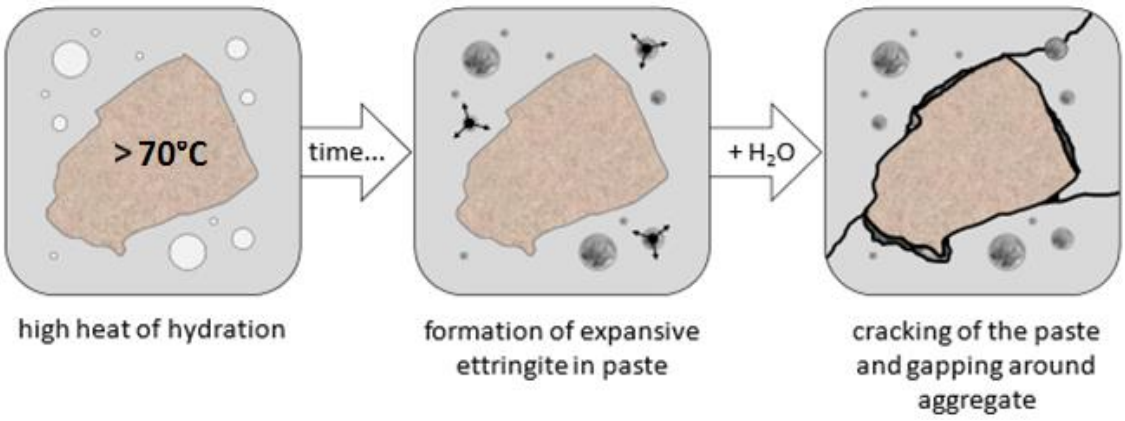

Figure 12: Delayed ettringite formation (Deschenes, 2009) adaptated

2.2.2.1 Mechanism of DEF

The ions necessary for the formation of etringite are present in practically any concrete solution and, in general, etringite crystals must be formed in a uniform manner, but some factors mentioned above hinder the process.

The expansion mechanism remains implies the effect of the crystallization pressure of etringite in the hardened concrete. The nature of the initial gel formed within these grouts is more of a dam effect, it can be seen simply as the effect of the empty filling of various needle-shaped objects, which is the configuration of the crystals. (MARTIN, 2012)

To explain the expansion mechanism, Taylor *et al.*(2001) is based on the physicochemical theory of crystal growth in porous materials developed by Scherer (1999). For Scherer (1999) the force that causes the growth of a crystal is provided by supersaturation and the maximum stress on the surrounding walls depends on the geometry of the crystal and the contour, causing significant pressure on the pore wall, only if its radius is smaller than about 100nm. The tension existing in a single pore, even when large, cannot cause the failure, as it acts on a very small volume of the material.

Taylor et al. (2001) it suggests that the formation of the crystals occurs as shown in Fig. 13.

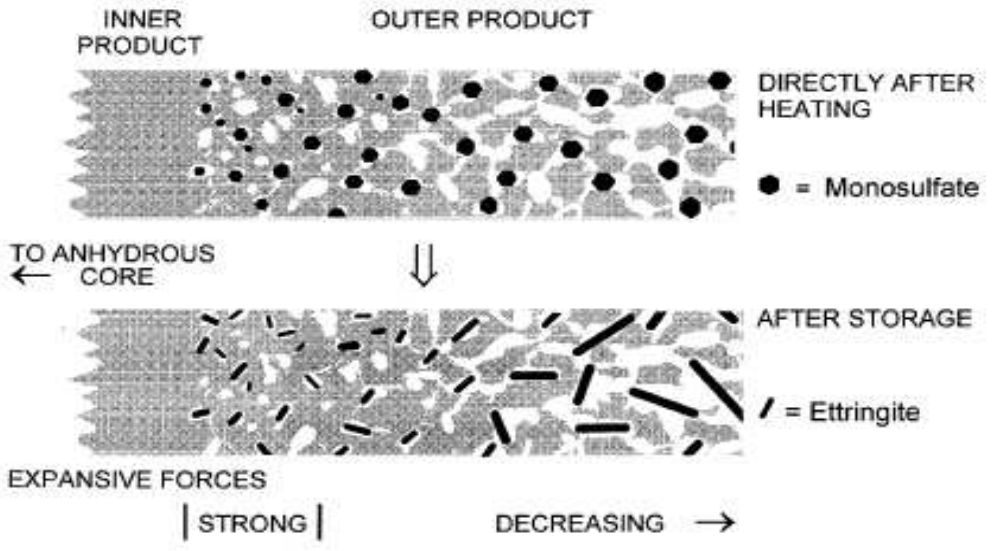

Figure 13: Representation of the formation of the etringite crystals (Taylor, *et al.* 2001)

In Fig 14 it is possible to see how the formation of the etringite crystals around the aggregate.

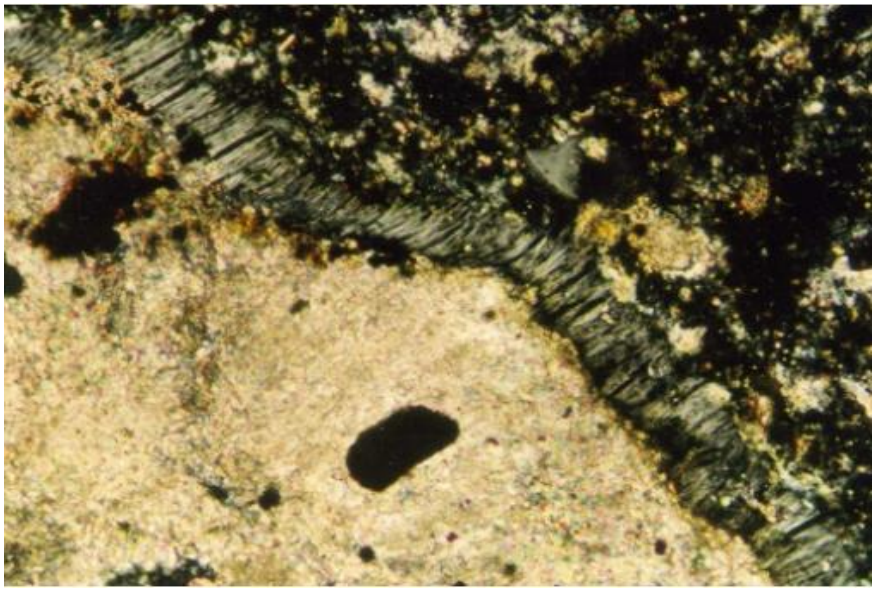

Figure 14: View of the concrete suffering from DEF as seen through a polarizing microscope showing a full separation of ettringite around an aggregated particle. (Ingham, 2012)

2.2.3 Main Parameters of Influence For The Occurrence Of Internal Swelling Reactions (ISR)

a) Alkali content:

Alkalis have strongly contributed to the development of internal swelling reactions. With regard to AAR they work not only as reagents for the formation of gel, but also to keep the internal pH high, creating an environment conducive to the development of the reaction. The greater the amount of alkali, the greater the expansion levels. According to Multon *et al.* (2007) in his study there was a decrease of about 70 to 80% of the expansion when the alkali content of mortar mixtures was reduced by about 50%, for the author, based on previous studies, an alkali content between 3 and 5 kg/m3 of concrete is recommended, because in this range or below it the expansion levels are small.

With regard to DEF, according to Brown and Bothe (1993), the presence of alkalis, such as sodium hydroxide, has a great influence on the stability of etringite, so that the higher the concentration of alkalis in the concrete mixture, the less stable is the etringite.

b) Humidity:

For the occurrence of AAR, water is a primary factor, as water works not only as a means of transport, but actively participates in the expansion process, considering that the silica gel absorbs water and expands. (MARTIN *et al.*, 2012)

Previous studies have shown that the constant or intermittent presence of water, as well as the high relative humidity of the air, in contact with concrete, is a necessary condition to delay the formation of primary etringite, favoring DEF. (PAVOINE *et al.*, 2006)

The expansion of both AAR and DEF is driven by the internal humidity of the concrete and the relative humidity of the air, by about 80-85% of the relative humidity (UR) for AAR and 90-92% for DEF, however these figures presented depend factors such as the type and nature of the concrete. With respect to AAR, the humidity provided by the mixture of a common concrete is usually high enough to generate expansion, unlike what happens with DEF. (MARTIN *et al*., 2012)

c) Temperature:

The rise in temperature inside concrete elements due to the heat of hydration can reach extremely high levels. According to Icenhower and Dove (2000), the solubility rate of silica increases exponentially with increasing temperature. The higher the temperature of the mixture during curing, the more soluble it will be in silica, favoring the formation of a hygroscopic gel from the alkali aggregate reaction. The silica will be more soluble the higher the temperature of the mixture during curing. As the hydration process and the drying of the concrete are essentially exothermic processes, it is difficult to control the effects of temperature with regard to the potential of AAR.

High temperatures alter the chemical reactions during cement hydration. For the formation of DEF, high temperature is a necessary and extremely important factor for this type of reaction to occur, so that the occurrence of this problem is more common in solid concrete elements or in concrete that has been subjected to heat treatment above 70°C. (PAVOINE *et al.*, 2006)

In relation to DEF the Figure 15 shows the difference in the behavior of a mortar cured at a high temperature and a mortar cured at room temperature. It is possible to observe that the expansion levels are very different between mortars.

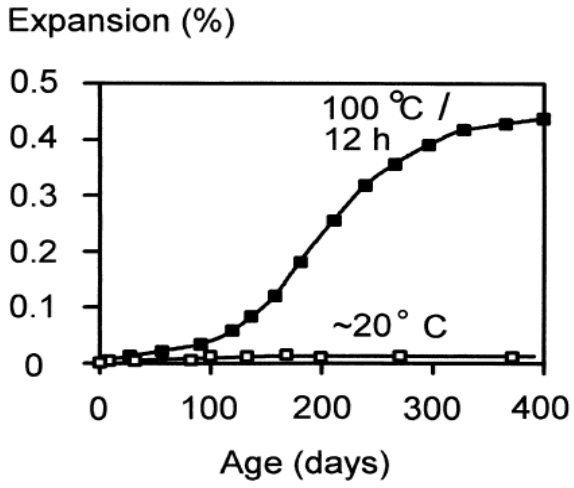

Figure 15: expansion curve of a mortar cured at 20° C and 100° C. (Taylor *et al.*, 2001)

d) Characteristics of aggregates:

The types of aggregates present in the concrete composition influence the occurrence of expansion reactions. Some aggregates are reactive, and the presence of reactive minerals is usually detected through petrography tests. Some are quickly reactive, while others react more slowly. Many rocks have silica as a component, but not all siliceous aggregates produce AAR. The reactivity or non-reactivity of the aggregates depends on their microstructure, that is, on the way they were formed geologically or mineralogically. (JURCUT, 2015)

The chemical composition of the aggregate and its characteristics define the amount of gel to be formed. The so-called *pessimum* effect may occur, where for a certain amount of alkali present in the mixture there are some reactive aggregates that potentiate the expansion. The aggregates have more influence when dealing with AAR and in this case the size of the aggregate should be considered. With respect to the DEF what should be taken into consideration and what is formed, which depending on the configuration forms a better interface, which helps to reduce the effects of thermal expansion. (MULTON, 2010)

e) Concrete porosity:

The porosity of concrete is an extremely important factor for the occurrence and development of both reactions. When the concrete presents a high degree of porosity the humidity enters the material more easily, besides boosting the mobility of the reaction reagents influences the degree of expansion. One factor to be considered is the degree of pore connection, i.e. if the porosity is open or closed, if the chance of moisture transport and other reagents increases. A decrease in the w/c ratio induces a decrease in porosity and corresponds to better mechanical properties, allowing the material to better support pressure. (MARTIN *et al.*, 2012)

2.2.4 Effects of ISR's on the mechanical properties of the Concrete

What justify the widespread use of concrete are its main mechanical properties: tensile strength, compressive strength and Young's module. These properties change when there are internal swelling reactions in the material. It is important to note that, under the conditions imposed in the laboratory to accelerate the onset of these reactions, the effects on these properties deviate somewhat from the real conditions, however, there is a consensus that internal reactions have a direct effect and significant impact on the mechanical properties of the material. (PIGNATELLI, 2012)

Before dealing with the effects caused by internal swelling reactions (AAR and DEF) on the concrete, it is important to say that both reactions can occur simultaneously, and that it is practically impossible to define which type of reaction affects the structure only with visual inspection, because the type of cracking resulting from these types of reactions are identical (Fig. 16 and Fig. 2-17). It is estimated that DEF occurs first

because of the hydration process, but in the literature there is no consensus on this, considering that with cracks resulting from the AAR the moisture can enter the structure and promote the re-crystallization of primary Etringite. (LARIVE, 1997)

Figure 16: ASR damage on barrier walls.
(Thomas et al, 2013)

Figure 17: Pier 6 of the Bellevue Bridge with map cracking in the tidal zone (DEF).
(Godart and Divet, 2013)

As mentioned briefly earlier, AAR and DEF cause cracks in the concrete, and the stress process caused by the expansion, whether by hydroscopic gel or etringite crystals, generally exceeds the concrete's tensile strength limit. Cracks have a direct impact, not only on the tensile strength, but on all the mechanical properties of concrete.

Through several studies by different authors [Ahmed, *et al.* (2003); Brunetaud *et al*. (2008); Giaccio *et al.* (2008); Lubej *et al*. (2014); Multon *et al.* (2005); Shayan (2016)

and Swamy & Al-Asali (1988)] it is possible to come up with the idea that internal expansions and cracking due to ASR / DEF can cause significant reductions in strength and other mechanical properties of concrete and lead to deterioration or even disintegration.

The magnitude of such problems depends on the severity of the reaction and the extent of expansion and cracking. In addition to the loss of compressive strength, the loss of tensile strength and young modulus is commonly attributed to the development of micro-cracks, and can occur well before significant expansion is measured.

The relationship between concrete expansion and micro cracking is different for each combination of materials, mix characteristics and environment. There is no number of decay of these properties as they depend on the type of concrete studied and even on the shape of the specimen, the only consensus that exists and that these reactions impact the mechanical properties of the material and significantly affect the durability of the material.

2.2.5 Diagnosis and Prognosis of ISR's in Concrete Structures

Thomas et al. (2013), Fournier et al. (2010) and Fournier & Bérubé (2000) provide guidelines for the diagnosis of internal reactions. Such reactions are recurrent and are largely responsible for the loss of premature stability of structures, therefore, combined on-site and laboratory tests are used to confirm the existence of internal swelling reactions. According to the cited authors, investigations are likely to include one or more of the following steps:

- Visual examination: The first step to be considered is visual inspection at the location where the structure is located; this inspection is carried out in order to identify whether the characteristics presented may result from internal expansion reactions. In this phase, factors related to the extent of deterioration are observed, in addition to the possibility of the presence of other degradation mechanisms, among others. The analysis of the place where the structure is located is also very important, as it is necessary to consider the conditions of exposure of the material.

- The in-situ monitoring of deterioration: After the visual inspections, the monitoring of the structure begins, where the levels of expansion, deformation and others will be observed. At this stage, it is also possible to remove the specimens that will be studied in the laboratory later.

- Laboratory tests: With the samples collected, various laboratory tests (including petrographic characterization, chemical, physical and mechanical tests) can be performed to diagnose the type of pathology found (AAR, DEF or both). A detailed petrographic evaluation is usually carried out to confirm the presence of

the alkali-silica reaction and to determine the nature of the aggregate if it is reactive. Many laboratory tests are also carried out to accelerate the onset of these reactions and to study the best ways to repair and monitor structures that present these pathologies.

After diagnosis, it is possible to find the best way to recover the structure.

2.3 USING OF FIBER OPTIC SENSOR FOR MONITORING CONCRETE STRUCTURES

Based on the growing need, new methods are being developed for the monitoring of concrete structures, among these new techniques is the use of fiber optic sensors (FOS). The study of this technology was initially applied to military and aerospace studies, but then it started to be studied how to incorporate this technique in civil engineering works. Although most studies related to the subject are applied to laboratory tests, it is possible to implement the use of optical fibers in real structures. (MERZBACHER *et al.*, 1999)

According to Mendez *et al.* (1990), pioneers in the study of fiber optic sensors incorporated into concrete, this type of technology can be easily applied to concrete, considering that optical fibers do not affect the properties of the material, as they have minimal dimensions, in addition to being material extremely sensitive to any variation that the concrete may present, such as thermal and size variation, that is, the fibers can provide accurate strain and temperature measurements. If fiber optic sensors are incorporated into the concrete at the time of construction, it is possible to investigate the internal condition of the concrete over time without damaging it.

The diversity of existing FO sensors makes a large number of applications possible. In fact, it is possible to measure displacements, deformations, stresses, pressures, optical indices, velocities (linear and angular), accelerations, temperatures and many other quantities thanks to different sensor configurations. (LI *et al.*, 2004)

The low intrusiveness of the fiber optic sensors makes them very useful in the SHM (Structural Heath Monitoring) sector: this involves in-situ monitoring of structures (buildings, bridges, civil engineering works) by integrating sensors in their center. This makes it possible, throughout the life of the structure in question, to monitor a multitude of parameters, in order to guarantee its integrity. (SABRI *et al.,* 2014)

2.3.1 Basic concepts about fiber optic sensors

According to Hisham (2018), optical fibers are basically an optical waveguide, which consists of the joining of filaments, which can be made of glass or polymers, and are

used as a means of propagating light. Optical fibers are basically composed of three layers: the core, the cladding, and the coating (Fig 18).

The core has a high refractive index and is coated with polymeric layers whose refractive index is lower, so that total internal reflection occurs and losses do not occur during the process. The cladding, in addition to protecting against losses, also works to protect the core from contaminants and incorporates mechanical resistance to the material. The coating is used to prevent the occurrence of physical damage, considering that it is a fragile material.

According to Merzbacher *et al.* (1999) for concrete, the correct polymer can also protect the glass fiber from the extremely alkaline environment (pH 12) which is corrosive to standard glass fiber.

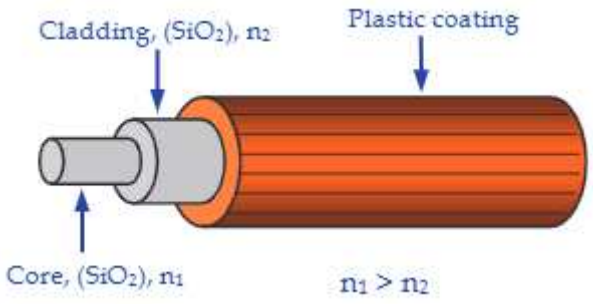

Figure 18: representation of a single fiber optic structure (Castrellon-Uribe, 2012)

2.3.1.1 Types of fiber optic sensors

Optical fibers have properties that allow for different approaches with regard to the design of optical sensors. Currently, there are several types of fiber optic sensors that can be classified into basically three different categories: locatlised sensors, distributed and multiplexed. These categories are based on the detection methods for each sensor. (KESAVAN *et al.*, 2010)

Lau (2003) describes these categories one by one as follows:

a) Localised sensors or point sensor: Localized sensors, as the name suggests, determine the use of a specific segment of an optical fiber, and are similar to voltage or temperature meters applied. The specific detection of the intensity modulation refers to the losses of light intensity that are directly related to the flexion or the micro curvature of optical fibers along any length extension. In this type of sensor, the active luminescent material at the distal end of the fiber responds to a temperature change applied to the optical fiber;

b) Distributed sensors: The sensors can be designed to be able to make measurements in a spatial way, that is, the variable to be measured can be determined along the length of the fiber itself, this type of method is called distributed detection. The distributed sensors make full use of optical fibers, as each element of the optical fiber is used for measurement and data transmission purposes. These sensors are more suitable for application in large structures, as they have multipoint measurement capabilities. A distributed sensor allows the measurement of a desired parameter as a function of length along the entire fiber;

c) Multiplexed sensors: Are generally built by combining several sensors to measure disturbances in a large structure, that is, the information is interpreted at specific points along the length of an optical fiber network. It is a complex technique where several researchers create innovative methods for the development of multiplexed fiber optic sensors. The most widely used multiplexed detection technique for measuring delays in the propagation time of light traveling in the fiber based on the change induced by measurement in light transmission. An optical time domain reflectometer (OTDR) is used primarily for this purpose. In this type of sensor, a pulsed light signal is transmitted to one end of the fiber, and the light signals reflected by several partial reflectors (splices) along the length of the fiber are recovered by the same end of the fiber.

The Figure 19 shows a scheme that represents these classifications

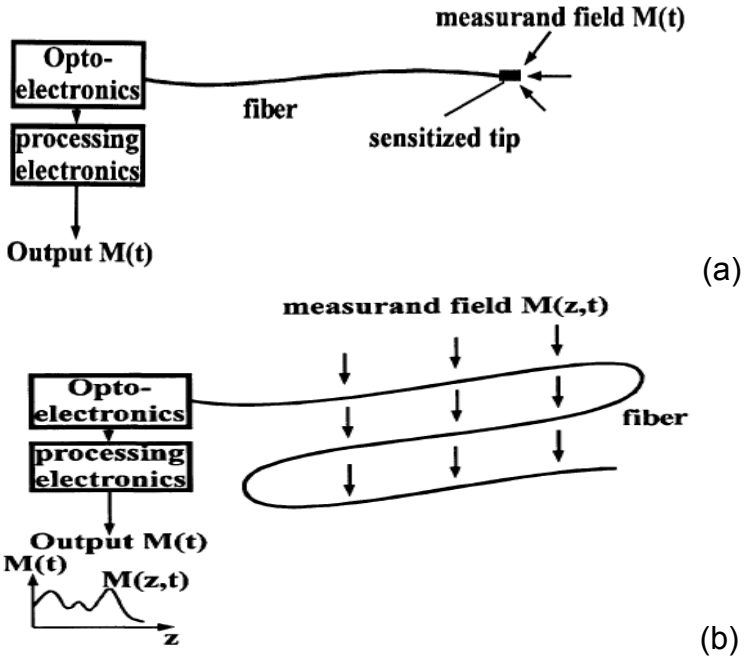

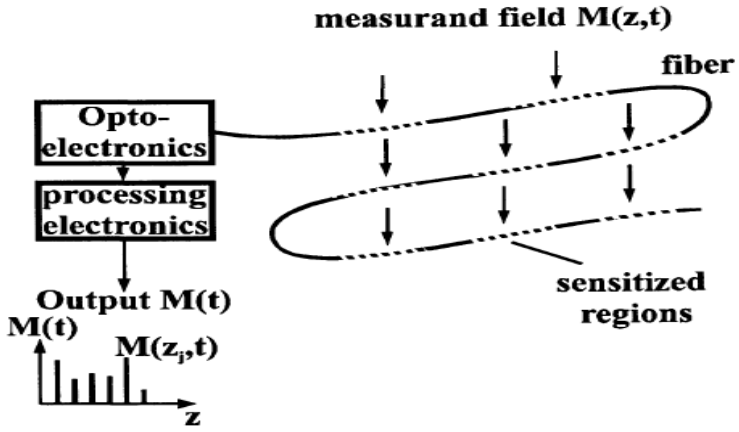

(c)

Figure 19: representative scheme of types of fiber optic sensors
(a) Localised (b) Distributed (c) Multiplexed.
(Grattan & Sun, 2000)

In a more simplified approach, sensors can also be classified into two major groups: extrinsic and intrinsic. (Fig. 20)

According to Michie (2000), when the fiber is used as a means of communication between the source and an external sensor, the sensor is known as the extrinsic sensor (EFOS) Fig. 20 (a). However, for most applications relevant to materials in the engineering field, the fiber itself will be used to perform the function of presenting variations along its entire length, in which case it is referred to as an intrinsic sensor (IFOS) Fig. 20 (b).

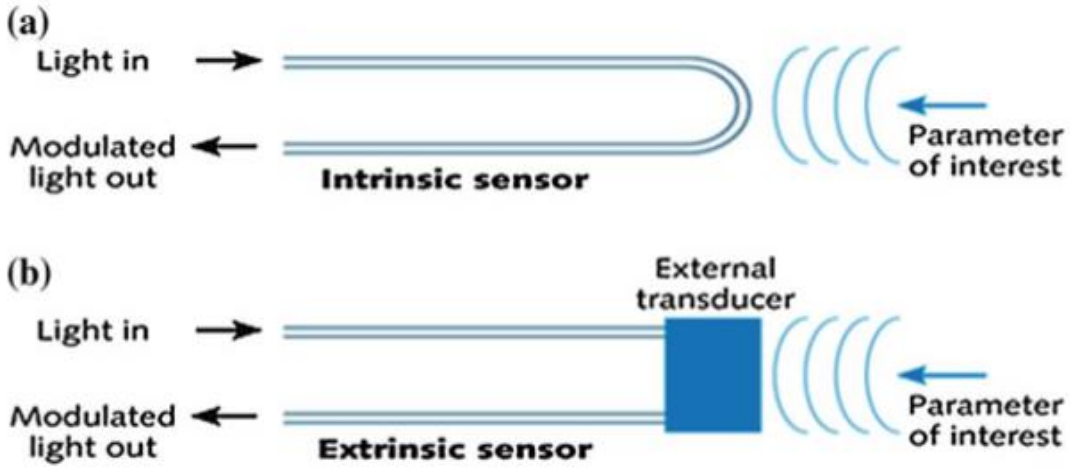

Figure 20: Classification of sensors: intrinsic devices (a) and extrinsic devices relay on a transducer (b)
(Sabri et al., 2014)

As noted, there are several types of optical fiber sensors used in engineering for the most diverse purposes, among them the extrinsic Fabry-Perot Interferometric (EFPI) sensors and the Fiber Bragg Grating (FBG) sensors are being used more for long-term / structural monitoring of concrete structures. (KESAVAN, 2010)

2.3.1.1.1 Fabry-Perot Interferometric sensor

The Fabry-perot fiber sensor is an in-line sensor device, which makes it very useful for a variety of applications. It is basically an optical cavity (called the FP cavity) that has high reflectivity mirrors with the reflective surfaces facing each other. Due to the high reflectivity, the transmission is spectrally selective and serves as an interference filter. (MEGGITT, 2010)

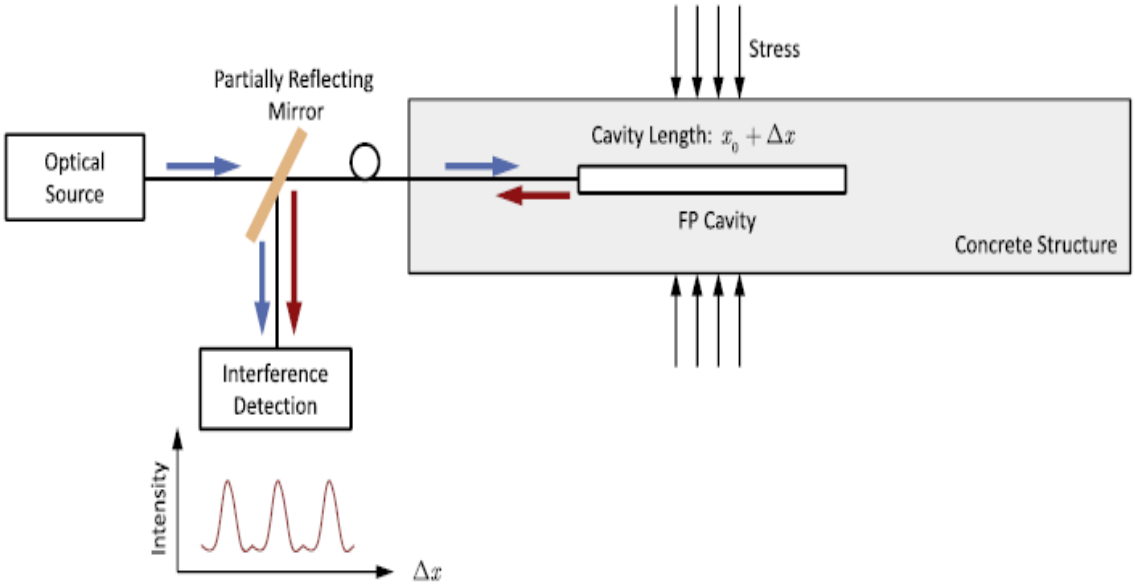

Figure 21: Fabry-Perot Interferometric sensor.
(Yehia *et al.*, 2014)

In sensors of this type, light is reflected partially at the sensor input and then again at the distal end of the sensor (Fig 21). If the light returning to the fiber entrance is in phase with the light being reflected at that point, constructive interference occurs. If the light is in the antiphase phase, destructive interference occurs. Adjusting the reflection coefficients at the sensor's final limits allows the sensor to be designed so that the light makes several passes. When all of these passages combine with the same phase, strong reflection occurs. (MICHIE, 2000)

According to Yehia et al. (2014) the optical cavity changes in length when any voltage is applied to the structure in which the FOS is inserted. From the moment the light is injected into the cavity, this change in length causes a change in the pattern of interference of the optical signal coming out of the sensor, linking the structural deformation to the variations received in the optical intensity. FP-based sensors are very sensitive to changes in the length of the optical cavity and therefore are more sensitive to small structural changes than other FOS techniques.

2.7.1.1.2 Fiber Bragg grating sensor

Among fiber optic sensors (FOS), Bragg fiber sensors, called FBG, are widely used and versatile. Basically, an FBG is a periodic variation in the refractive index along the fiber. This variation occurs due to the exposure of the nucleus to an intense pattern of optical interference. TAHERI (2009)

Generally speaking, the FBG's monitoring system consists of monitoring the wave of the "Bragg" response signal as a function of the variable being measured, such as temperature, voltage and others. The system has gratings in its composition (Fig. 22), which are a fundamental part of this type of sensor, because when a spectral source injects light into the fiber, these are Bragg grating that reflect, in response, a narrow spectral component corresponding to the measurement performed by each grating (Fig 23). (GRATTAN & SUN, 2000)

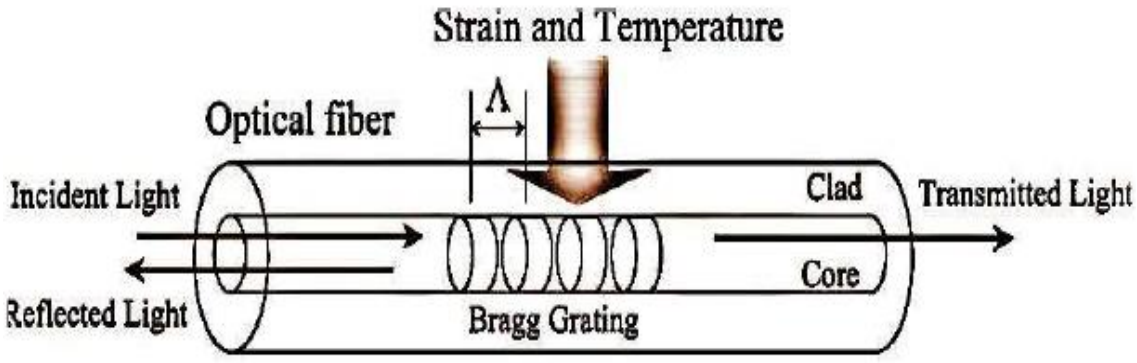

Figure 22: representative scheme of Fiber Bragg grating.
(Ramakrishnan et al., 2016)

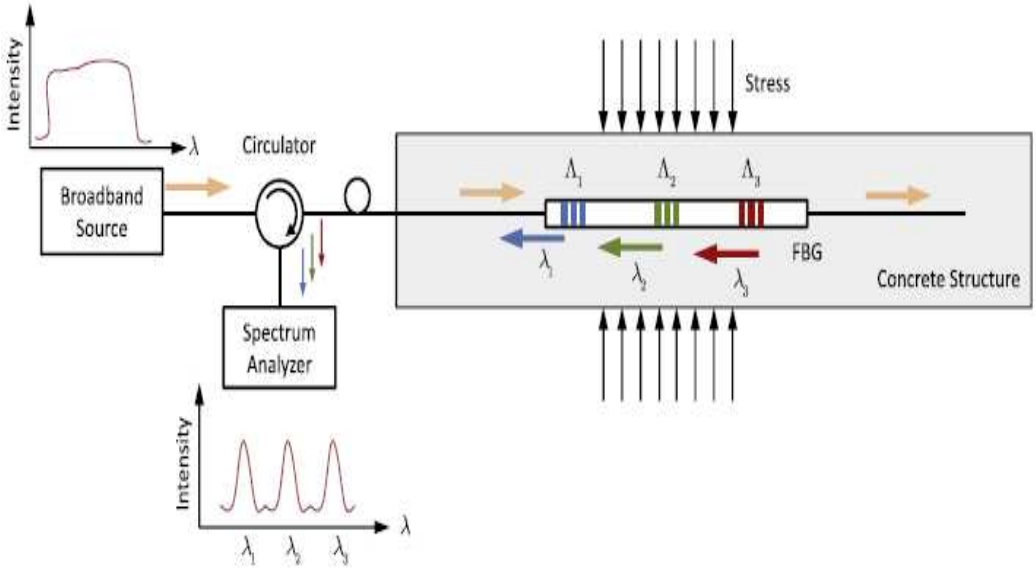

Figure 23: sensor representation of Fiber Bragg grating in a concrete element.
(Yehia *et al.*, 2014)

The equation 6 represents the reflected light due to periodic variations in the refractive index of the Bragg grid with a central wavelength, where n_0 is the effective refractive index of the guided mode in the fiber core and ∧ is the grating pitch.

$$\lambda_B = 2n_0\Lambda \quad (6)$$

Pei *et al.* (2014) says that the main reason why FBGs are widely used is that, through this type of sensors, temperature and tension can be measured at a series of points along a fiber line, and have several advantages over conventional sensors.

2.3.2 Problems for the application of fiber optic sensors

Although fiber optics sensors are being successfully applied to several types of structures, Deng and Cai (2007) have some problems with the application of FOS's that still need further investigation. The main problems listed are:

a) Strain and temperature discrimination: Some sensors are highly sensitive to deformations and temperature variations at the same time (this is the case with FBG sensors), so that it is possible to obtain deformation values, the change in wavelength caused by tension and temperature must be separated. Often, to solve the problem, temperature sensors are used and after the readings, compensations are made to separate the two quantities;

b) Effects of coating materials on strain measurement: Normally the fiber's protective coating, is made of plastic in order to protect the fiber core, due to its fragility, however these coatings can absorb deformations causing the fibers to detect only a portion of the stresses generated by the deformation structure;

c) The bonding of Fiber Optic Sensors: The efficiency of the readings through the sensors can be reduced depending on the poor anchoring of the fiber to the material, so, the effective bonding between FOSs and the host materials is particularly important.

The problems listed by Deng & Cai (2007) and many others must be taken into account before applying optical fiber sensors to solve engineering problems, thus seeking the best way for an efficient application.

2.3.3 Practical application of fiber optic sensors in concrete structures to measure internal changes.

According to Bao et al. (2010) in the case of concrete structures, there are numerous places where cracks can occur, so that, in order to analyze the structure in a global way, the use of localized sensors becomes impractical, as it would require a very large number of point sensors, in this case, it becomes more appropriate to use sensors distributed as shown in Figure 24.

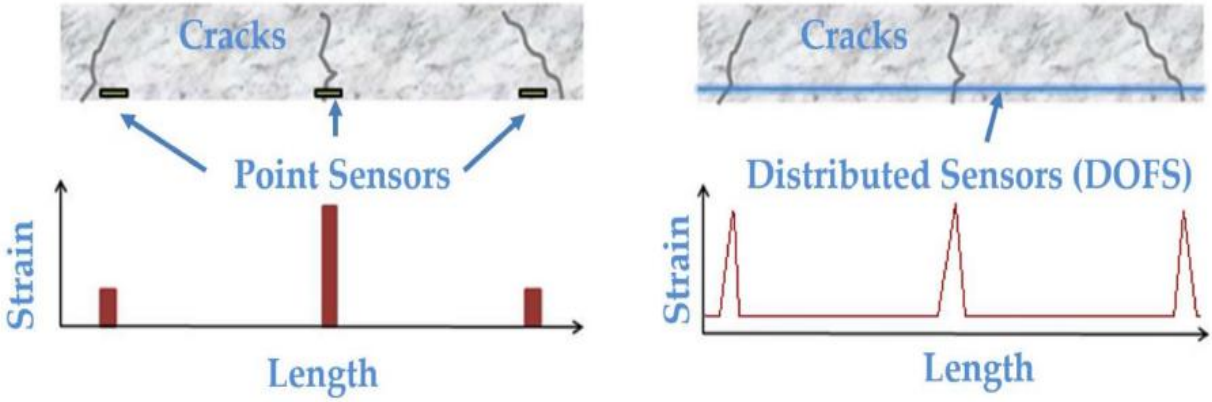

Figure 24: distributed sensor for crack detection.
(Barrias *et al.*, 2018)

2.3.3.1 Applications to Crack Monitoring

To detect cracks in concrete elements, several authors [Leung (2001); Wan and Leung (2007); Bao et al. (2010); Mahdikhani & Bayati (2008)] present the "zigzag" method. This method consists of inserting the fiber with a certain inclination in the structure (Fig. 25 a). Before the cracks appear, the distribution of the light intensity along the fiber is measured. When a crack opens in the structure, the fiber bends to remain continuous and, consequently, the light intensity is changed. Backscattered power is measured as a function of time with optical time domain reflectometry. Before the formation of cracks, the backscattered signal versus time follows a relatively smooth curve (Fig. 25 b).

When there are cracks in the path, there is a gradual loss of signal strength over time, this is due to the increased distance traveled by the light signal. When a crack opens in the structure, a fiber that intercepts the crack at an angle other than 90 ° needs to bend to remain continuous, using the optical power loss curve versus crack opening at the angle of inclination of the fiber to the crack, it is possible to determine the crack openings. It is possible to use a single fiber to detect and monitor multiple cracks. This is

because any point along the fiber has detection capability. As the fiber has a distributed crack detection capability, the crack location does not need to be known a priori.

This angle of inclination of the fiber is very important because the crack openings can only be determined with the power loss curve versus crack opening at this angle.

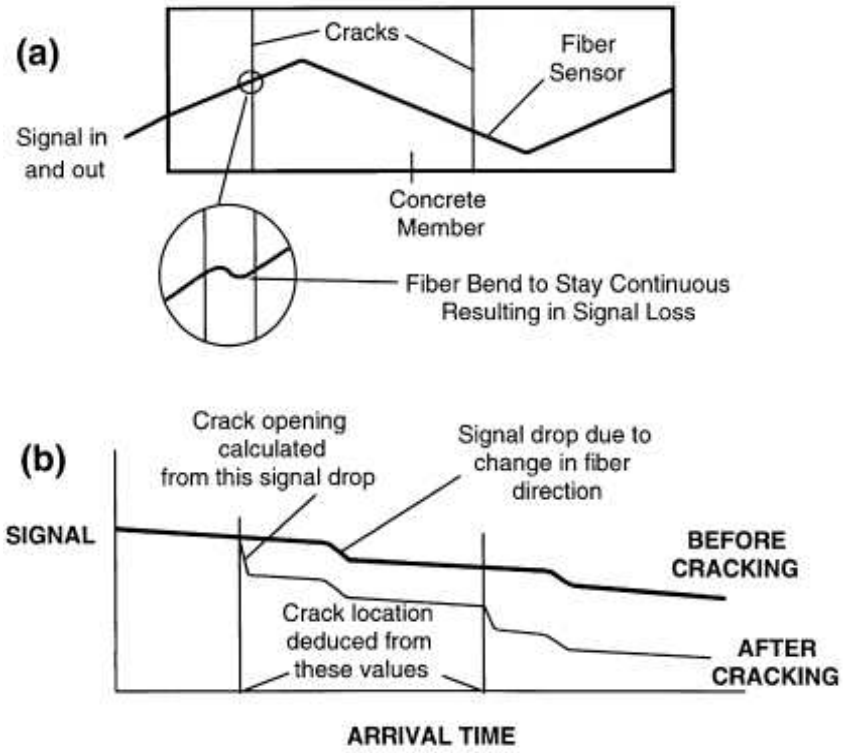

Figure 25: representation of the crack detection principle (Leung, 2001)

2.3.3.2 Laboratory tests and on-site application of FOS on concrete structural elements

2.3.3.2.1 Strain, crack and temperature monitoring

Although the use of optical fiber sensors has numerous advantages, as it is a technology with recent application in the field of civil construction, mainly for the study of concrete, it is still a little explored field in laboratory and field tests. In this regard, one of the main challenges in the use of these sensors is the relationship between the precision in measuring the deformation data of the material monitored in the laboratory and the protection and durability achievable of a sensor when exposed to natural environmental conditions in applications in structures real. (BARRIAS, 2018)

The work of Mendez *et al.* (1993) is one of the first records of laboratory tests performed with the insertion of optical fibers in cementitious materials. One of the initial concerns of this work was the adhesion between the optical fiber and the cement paste, it was observed that materials made only with cement paste does not provide a good

adhesion, however, heterogeneous and composite materials such as concrete, present a better adhesion due to presence of sand and coarse aggregates in its composition.

The test carried out by Mendez *et al*. (1993) consisted of inserting fibers optical in the concrete before curing the material, in this test the fiber optical was placed in a cylindrical sample in the direction perpendicular to the load that would be applied later, in another specimen the optical fiber was placed in the direction parallel to the applied load, as shown in Figure 26.

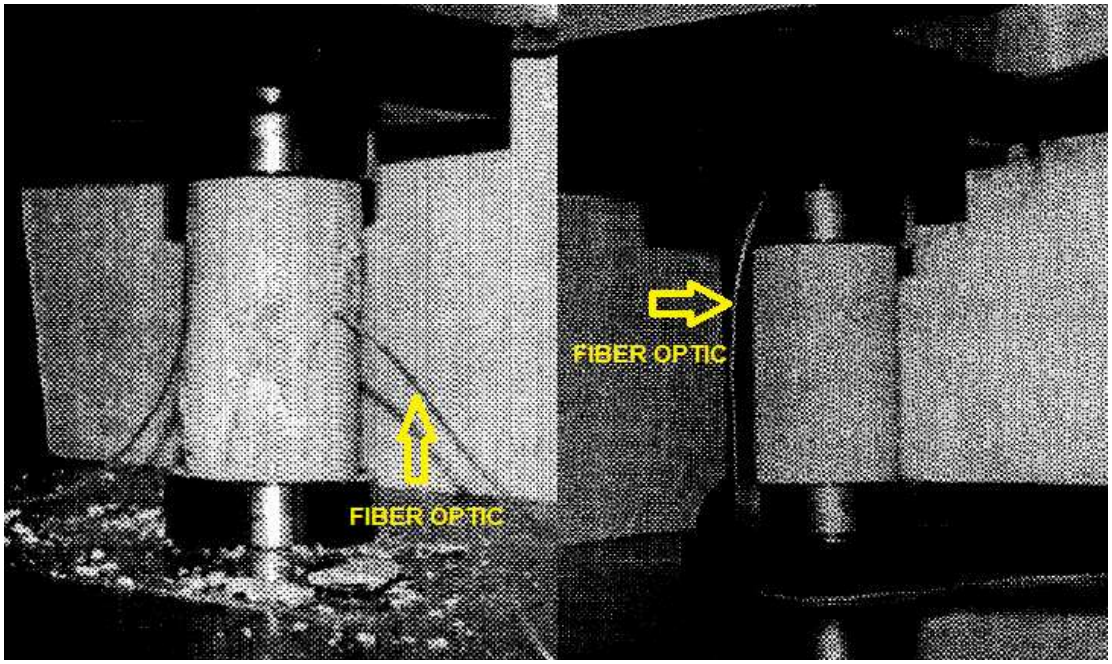

Figure 26: Fiber optics sensors inside the concrete samples (Mendez *et al.*, 1993) adaptated

It was observed that when the fiber was placed in the direction perpendicular to the load, the light intensity through the fiber remained stable until the rupture of the cylinder, since when the fiber was placed parallel to the direction of the applied load, the situation changes drastically, so that the light intensity begins to decrease shortly after stress begins to accumulate within the sample.

After the cylinder experiences the first shear crack failure, the power loss becomes stable again until more tension builds up again and another partial shear failure occurs, at which point the power drops again and the whole process repeats for the third time until the sample disintegrates under the excessive load, showing that the direction of the fibers directly interferes with the detection of cracks in this type of material.The test by Mendez et al. (1993), although it was one of the first, brought important advances in the study of the use of optical fibers in the detection of cracks in concrete.

As time went by the interest in concrete tests using fiber optic sensors increased and more tests were carried out to analyze the potential of this technology in the study of the material, as is the case of studies carried out by Yehia *et al.* (2014)

The work developed by Yehia *et al*. (2014) used optical fibers to measure deformations due to physical changes, such as heat of hydration, as well as deformations due to cyclical and torsional loads. Concrete cylinders of 15x30cm and beams of 175cm in length and with a cross section of 35 x 55cm were used. Fiber optic sensors were inserted in the cylinders (1 in each) and in the beams (2 in each) as shown in Figure 27.

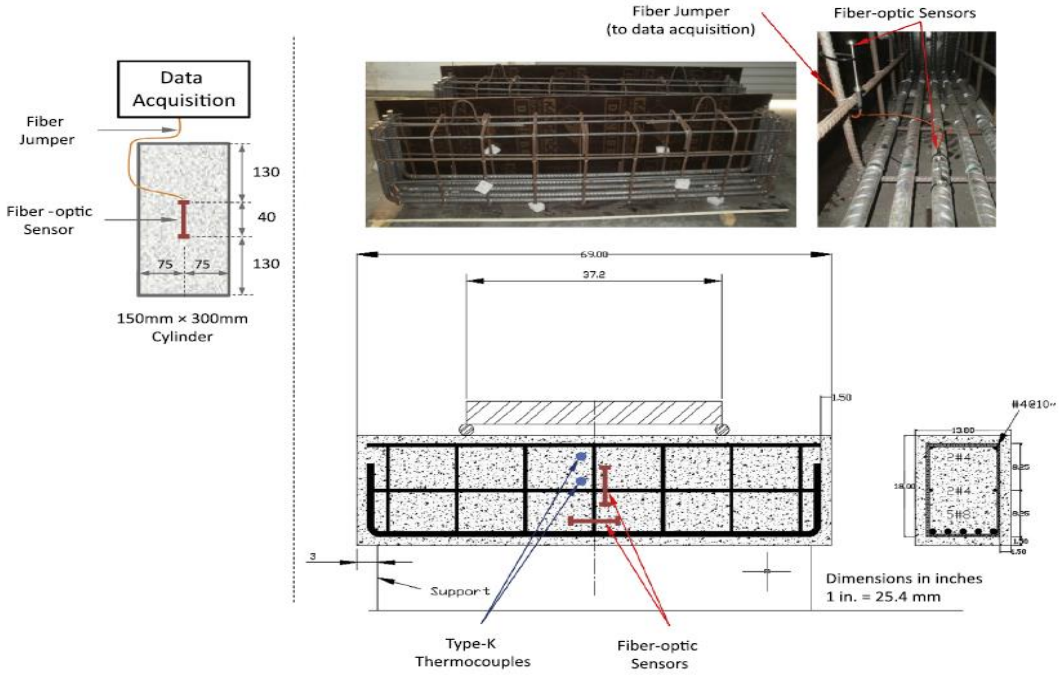

Figure 27: Experimental setup: cylinder and beam testing.
(Yehia *et al.*, 2014)

The FOS sensors used in the experimental investigation were the embedded fiber optics sensors, temperature-compensated strain gauge for cylinder and beam testing, respectively. The sensors are based on Fabry–Perot interferometry.

To identify temperature variations during the hydration of the concrete, thermocouples were incorporated in the middle and on the surface of the beams, the embedded sensors could detect temperatures between 40°C and 100°C. All sensors were connected to the data acquisition system right after molding to record deformations due to the heat of hydration and also the shrinkage of concrete. The same procedure was used for both beams and cylindrical specimens. Monitoring was done continuously for 7 days. In the Figure 28, it is possible to observe the performance of tests with cylindrical samples and concrete beams.

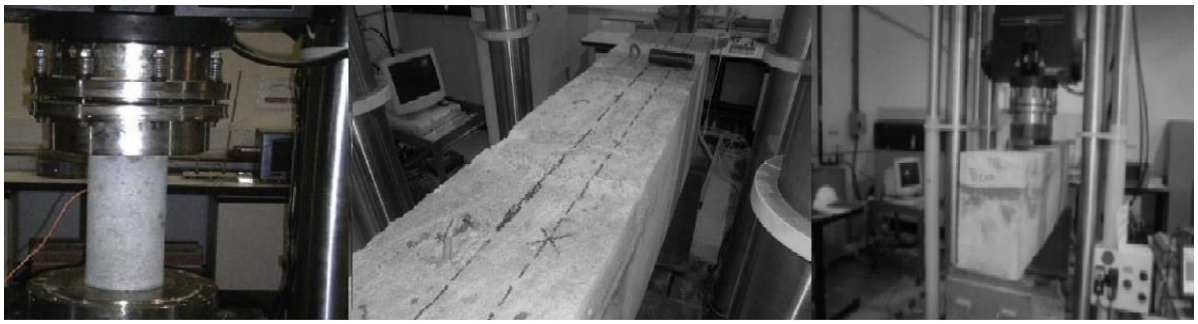

Figure 28: cylindrical sample and beam during the tests
(Yehia *et al.*, 2014)

In the figures 29, 30 and 31 it is possible to see the results provided by the sensors, for each test performed on the concrete samples, as a function of time.

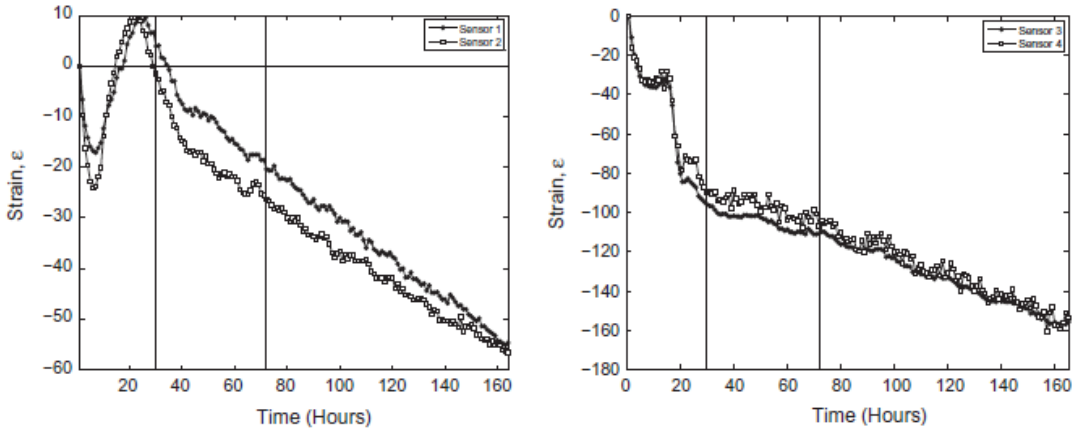

Figure 29: FOS deformation results in the four cylindrical concrete samples
(Yehia *et al.*, 2014)

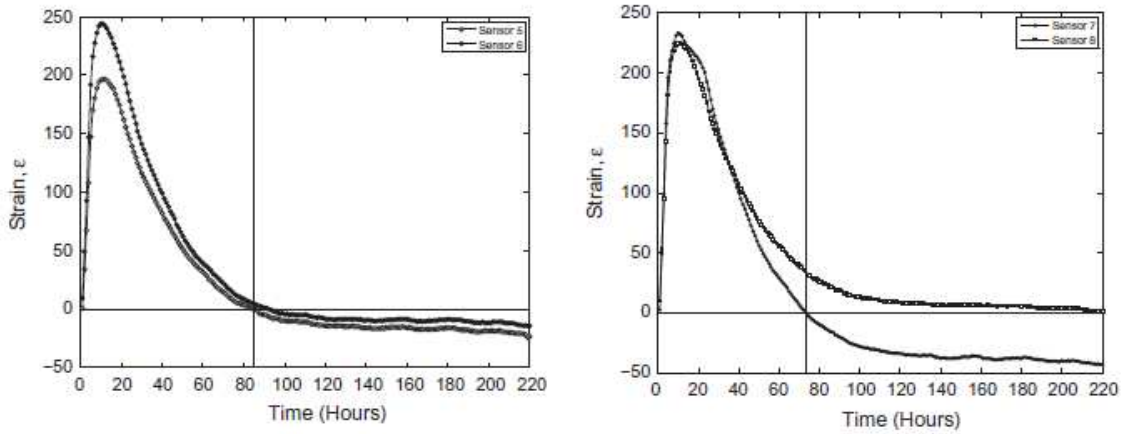

Figure 30: FOS deformation results in beams
(Yehia *et al.*, 2014)

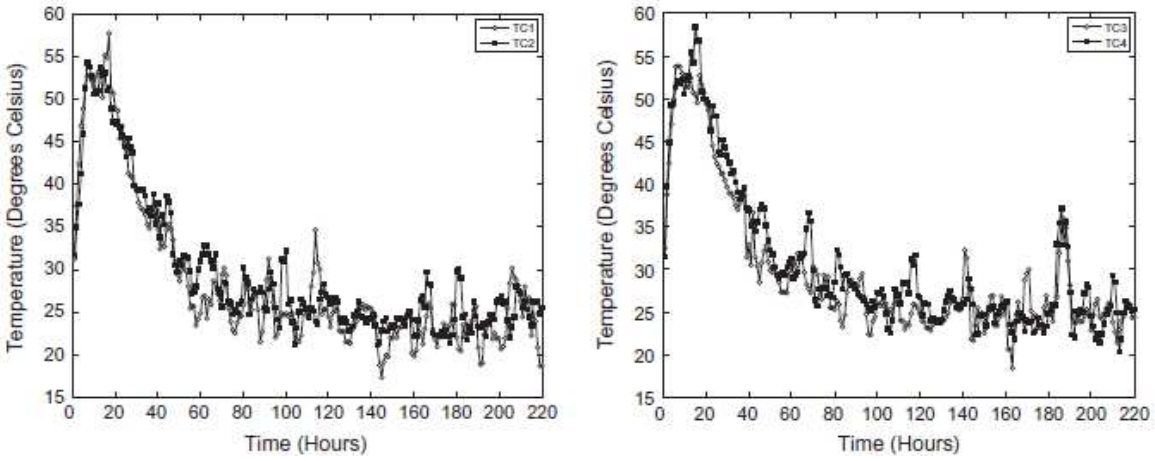

Figure 31: Temperature variation in beams presented by thermocouples (Yehia *et al.*, 2014)

As a result, in the test made by Yehia it was possible to observe in all tests, the FOS sensors showed instantaneous response to any changes in loading as well as temperature changes, which indicate the sensitivity and the ability of the FOS sensors to record responses from the samples of concrete due to loading or during hydration and shrinkage of plastic / drying.

The work of Yu Ge *et al*. (2014) analyses the response of strain sensors embedded in concrete beams subjected to thermal loading, where different types of fiber optic sensors are used. The instrumentation of sensors in the concrete beam is shown in the Figure 32.

In this study (Yu Ge *et al.*, 2014) the measurements were made over a period of 95 hours. The test was developed in two stages, the first with constant temperature and the other with variation (temperature gradient). The maximum temperature applied to the box responsible for heating the beam was 46 ° C.

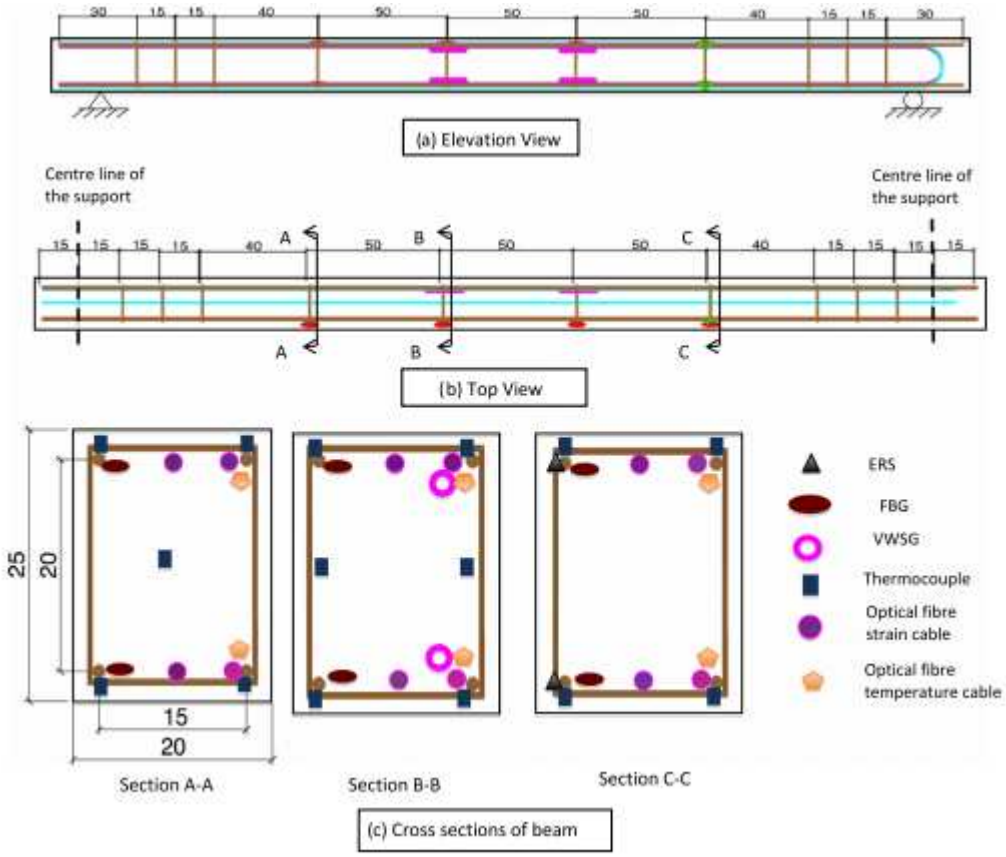

Figure 32: sensor instrumentation
(Yu Ge *et al.*, 2014)

The Figures 33 and 34 show, respectively, the results of temperature measurements and deformation measurements due to thermal action before and after temperature compensation.

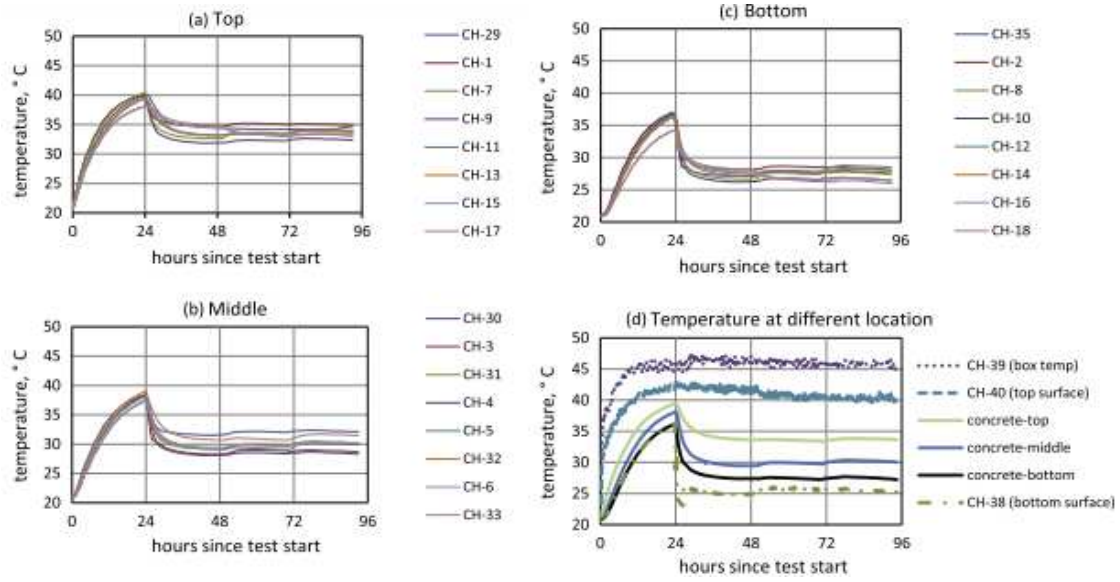

Figure 33: Temperature gradient through beam depth
(Yu Ge *et al.*, 2014)

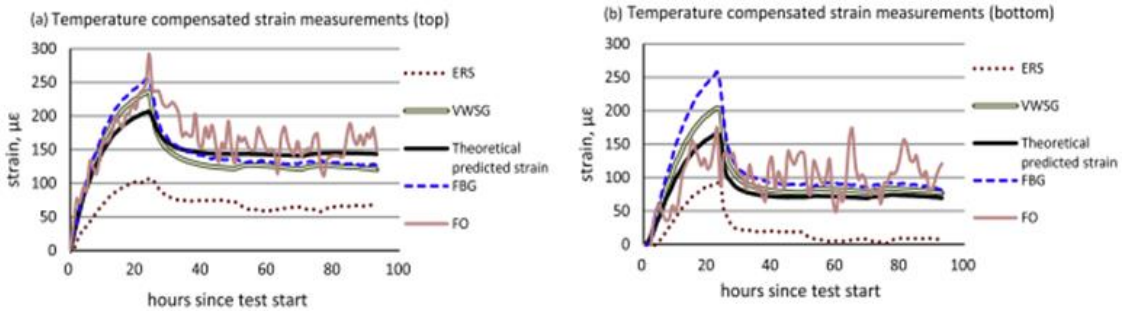

Figure 34: Strain measurements of instruments inside the concrete beam subjected to dynamic temperature environment.
(Yu Ge *et al.*, 2014)

According Yu Ge *et al.* (2014) from the comparison of the results that included compensation for the effects of temperature, following the directions of the sensor manufacturers, it demonstrated an average variation of 25% in measurements between the different types of sensors under the constant temperature test. For the temperature gradient test, an even greater variation (30%) in the measurements was observed.

2.3.3.2.2 ISR's monitoring

One of the works that uses FOS to analyze one of the internal swelling reactions (in this case AAR) is the work of Dunant & Scrivener (2012). In this work it was performed an experimental study using sensors embedded in reactive and non-reactive concrete samples, with the samples loaded in modified creep frames.

In the concrete mixture procedures, reactive and no-reactive coarse aggregate were used. The concrete was cured at a temperature of 20° for 28 days. After that time the concrete was placed in a room with a controlled temperature of 38°. It is important to highlight that the reaction (ASR) was not accelerated. After this cure, the samples were placed in creep frames and subjected to 0, 5, 10 and 15 MPa stress levels.

Three standard cylindrical concrete specimens - height 335 mm, diameter 160 mm – were loaded in creep. In each column: a non-reactive sample on top and two reactive samples at the bottom (Fig. 35). The load in each column was kept constant by hydraulic pressure, and the non-reactive samples allowed us to distinguish strains due to creep from the expansion induced by ASR.

Figure 35: Samples in the loading frame
(Dunant & Scrivener, 2012)

For FOS monitoring, the sensors embedded in each sample placed in the loading frame were: A temperature sensor (the temperature sensor allows the correction of small strain fluctuations due to variations of the ambient temperature); The elongation is measured using a Fiber Bragg grating sensor (length 67.5 mm); A longitudinal strain gauge (optical fibre length 100 mm) which functions in the same way as described above, but without a temperature sensor; A computer which logged the sensor values every 20 min.The resolution of both captors is 0.001 mm.

The scheme for installing the sensors in concrete is shown in Figure 36. During the tests the samples were undisturbed and strain variations due to temperature fluctuations could be compensated. The low dispersion can be explained by the scale at which cracking occurred. As the aggregates used are slow reacting aggregates, the cracks caused by the reaction are all micro-cracks in the aggregates and in the cement paste. No macroscopic cracks were observed at the surface of the samples during the duration of the experiments.

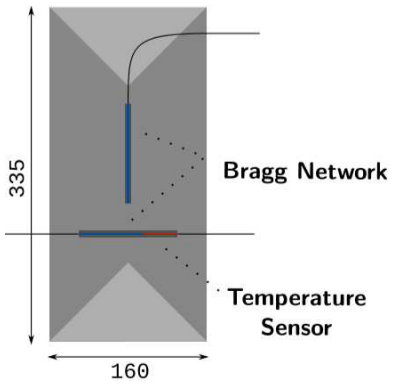

Figure 36: Schematic of the sample instrumentation.
(Dunant & Scrivener, 2012)

The Figure 37 (a and b) show how deformations occur, both due to the applied loads and the presence of ASR, simultaneously. Under load, a clear direction of propagation is favored: parallel to the load. When the load is further increased, the longitudinal expansion goes to 0, but the lateral expansion increases. This behavior is at odds with the idea of a "redistribution" of the expansion.

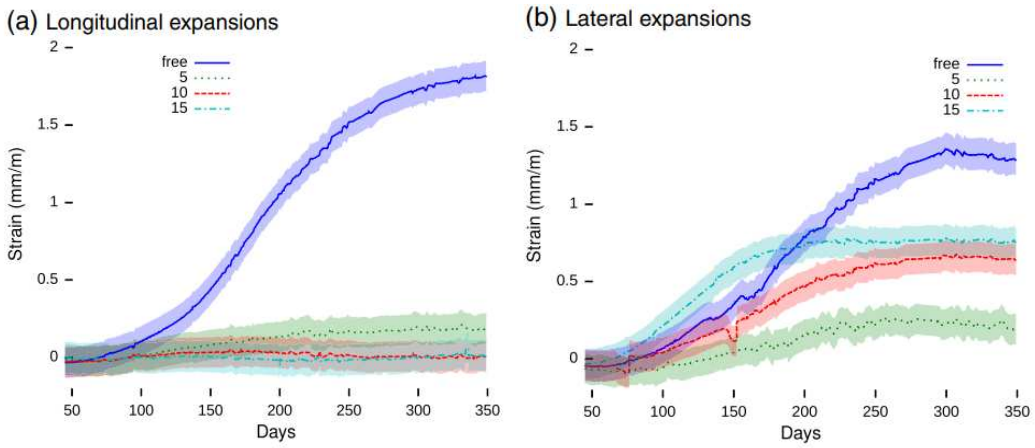

Figure 37: (a) Longitudinal and (b) Lateral expansions of samples due to ASR and load application.
(Dunant & Scrivener, 2012)

Under the 5 MPa stress level, the cracking is more pronounced and its onset began often on the aggregate. Notable features of the crack patterns are that damage concentration are immediately around gel pockets, a network of cracks connecting the gel pockets. A dense pattern of short radial cracks immediately around the aggregates and relatively few main cracks which will grow to the edge of the samples.

The effects of uni-axial stress on the expansion of ASR reactive concrete were linked to the orientation and development of micro-cracks in the aggregates and paste. It is notably found that the expansion is not redistributed, but the applied load forces the orientation of the micro-cracks at the micro-structural level.

The expansions observed experimentally at 5 MPa is probably due to the very specific combination of mechanical properties of the materials, the aggregate type and the morphology of the cracks formed. As the strength of the material was not measured, this result does not indicate that the concrete is less damaged at this load.

3 EXPERIMENTAL PROCEDURE

The experimental program was carried out in order to verify the feasibility of using fiber optic sensors in order to measure expansions in concrete elements resulting from Shrinkage and internal swelling reactions (ISR).

The specimens were designed in such a way that their dimensions are in accordance with RILEM AAR-4 (2016), which presents guidelines for the execution of tests in the laboratory which aims to accelerate the occurrence of internal swelling reactions, in this case the alkali-aggregate reaction.

This chapter presents the methodology developed in the work, the execution protocol followed, the materials used, equipment and software, concreting and the methods adopted. Also, in this item, the general methodology used to analyze the collected data is described. The experimental program for this dissertation was developed at the Institut Catholique d'arts et Métiers (ICAM – site Nantes/FR) laboratories.

3.1 PROTOCOL

The protocol of this study consists of making 3 concrete prisms with dimensions of 75 X 75 X 285 mm. Of these 3 prisms, 2 will be placed in conditions favorable (temperature, alkaline solution and others) the occurence of internal swelling reactions, in this case AAR, following the recommendations established by the RILEM AAR-4 (2016): Detection of Potential Alkali-Reactivity -Test Method for Aggregate Combinations Using Concrete Prisms, and 1 prism will remain under normal environmental conditions.

The aim of promoting the occurence of AAR was due to the fact that, on a macroscopic scale, the expansion effects for AAR and DEF are identical.

Fiber Optics sensors, type FBG, and sensors of temperature PT100 will be placed inside each prism, in order to measure expansions or dimensional changes in the material, due to internal swelling reactions (in the prisms exposed to the aggressive environment) or shrinkage effects (in the prism that will remain under normal environmental conditions).

The optical signal emitting equipment (BraggMETER) which will be presented in detail in section 3.2.3, has 4 channels, which can be used simultaneously. In this case, 3 channels should be used for the sensors placed inside the concrete and 1 channel in which the optical fiber should be kept under normal conditions for calibrating the device and measuring the parameters of the fiber exposed to air only, which justifies the amount of prisms defined in this experimental protocol.

3.2 MATERIALS

3.2.1 Concrete

The choice of materials is an extremely important step, as the goal is to induce ISR's in a short time, so the choice of materials for making concrete was made according to the guidelines presented by RILEM AAR-4 (2016) which determines which materials should be used in laboratory tests capable of accelerating the occurance of internal swelling reactions in this type of material.

The constituent materials of the manufactured concrete, as well as their characteristics, are presented in detail below.

3.2.1.1 Cement

The cement recommended by RILEM AAR-4 (2016) is the CEM I type for having a high clinker content in its composition.The cement used for this study was CEM I 52.5 R. According to NF EN 197-1 (2012) this is a cement that has between 95 and 100% clinker in its composition, which directly influences this type of experimental test, because it has a higher concentration of alkalis, present in clinker, in addition it is a cement that, when compared to other types, releases more heat at the time of hydration. The characteristics of the cement used are shown in Tables 1, 2 and 3.

Physical and Mechanical Properties of the used Cement	
Especific Gravity (g/cm³)	3,13
Blaine Specific Surface (cm²/g)	4.120
Initial Setting Time (min)	135
Volume Expansion (mm)	0,8
Water Absorption Ratio by weight (%)	28,8
1 Day Compressive Strenght (MPa)	26,9
2 Days Compressive Strenght (MPa)	40,2
7 Days Compressive Strenght (MPa)	-
28 Days Compressive Strenght (MPa)	72,4

Table 1 – Physical and Mechanical Properties of the CEM I 52.5 R (Provided by the manufacturer, 2020)

Chemical characteristics of the used cement	
SO_3 (%)	3,48
CL^- (%)	<0,10
Loss on Ignition (950°C)	0,33
S^- (%)	<0,10
Alkalis [Na_2O + 0,658 K_2O] (%)	0,24

Table 2 – Chemical composition of the CEM I 52.5 R (Provided by the manufacturer, 2020)

Constituints of the used cement	
Clinker	**95%**
C_3S (%)	66,7
C_2S (%)	11,6
C_3A (%)	8,6
C_4AF (%)	8
Limestone	**5%**

Table 3 – Composition of the CEM I 52.5 R according mineral phases (Provided by the manufacturer, 2020)

The CEM I (EN 197-1) used corresponds, in terms of composition, to the cement defined by the Brazilian standard NBR 16697-2018 as CPV-ARI. Both cements have a high percentage of clinquer in their composition and are free of additions. Regarding the compressive strength, the CEM I, according to the information provided by the manufacturer contained in Table 1, presents a compressive strength above and 70 MPa at 28 days, a result hardly obtained by CPV-ARI, which shows that the cement used is, in general, a greater strength than the Brazilian cement. This correlation is important, bearing in mind that in the next sessions of this chapter, it is noted that materials of Brazilian origin were used in order to establish a test that would be compatible with the Brazilian reality regarding the internal swelling reactions, due the high incidence of this type of expansive reaction in the country.

3.2.1.2 Sand

The sand used in the manufacture of concrete was a thick natural sand sold in bags and from the city of Recife, in Brazil. The particle-size characteristics of the sand were obtained through the granulometry test described by ABNT NBR NM 248: 2003. The particle-size composition of the material is described in detail in Figure 38.

The determination of the unit mass of the sand used was made according to ABNT NBR NM 45: 2006. In general, the sand used for making the concrete presented the following characteristics:

Unit Mass = 1.59 g/cm^3

Maximum particle-size = 4,75mm

Fineness modulus = 2,57

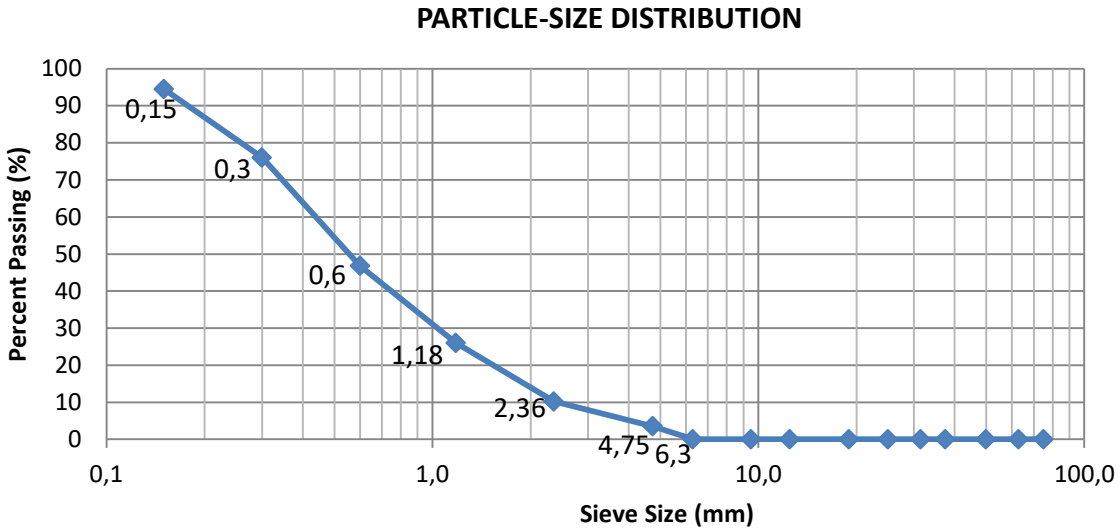

Figure 38: Particle-size distribution of sand (Author, 2020)

3.2.1.3 Coarse Aggregate

The coarse aggregate used in this study comes from a quarry located in Pernambuco/Brazil. For physical characterization, the test described by ABNT NBR NM 248: 2003 and specific mass test was performed. The particle-size distribution of the material is described in detail in Figure 41. In general, the sand used for making the concrete presented the following characteristics:

Maximum particle-size = 19 mm (Fig. 39 and Fig. 40)

Unit mass in the dry compacted state = 1,379 g/cm^3.

Figure 39: Granulometry test of coarse aggregates
(Author, 2020)

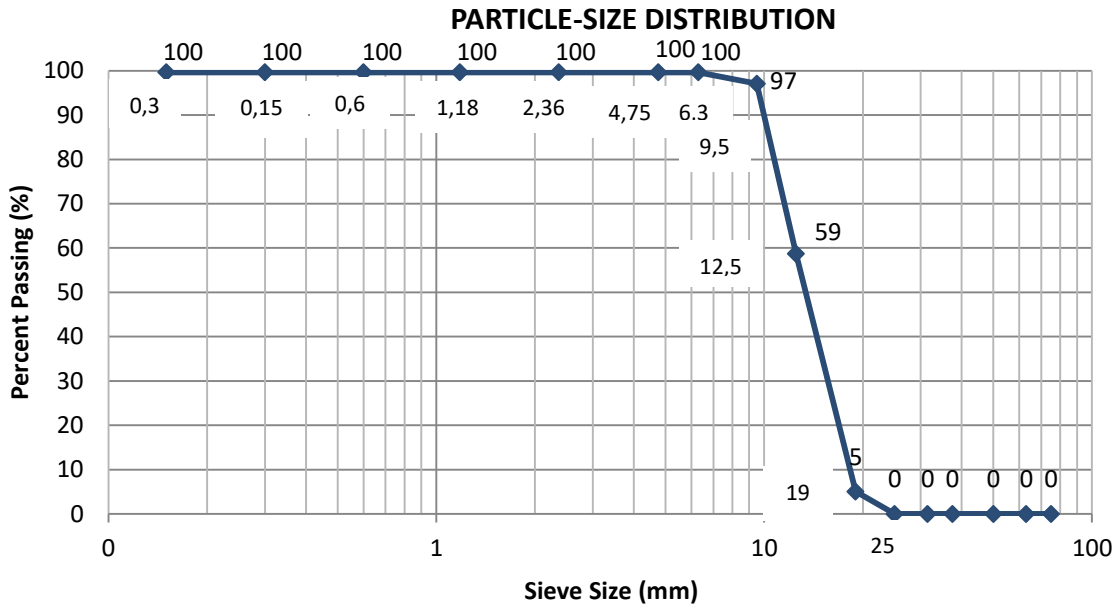

Figure 40: Particle-size distribution of coarse aggregate
(Author, 2020)

It is important to note that the coarse aggregate used has the same origin as the aggregate used in the Marins (2021) study. The Marins (2021) study proved the potentially reactive nature of the aggregate by the petrography test (Fig. 41), following the criteria established by RILEM AAR 1.1 (2016) and ABNT NBR 15577-3 (2018). The aggregate was classified as potentially reactive aggregate containing Quartz. The reactive nature of the aggregate was later confirmed by Marins (2021) through experimental tests defined by RILLEM AAR-4.1 (2016).

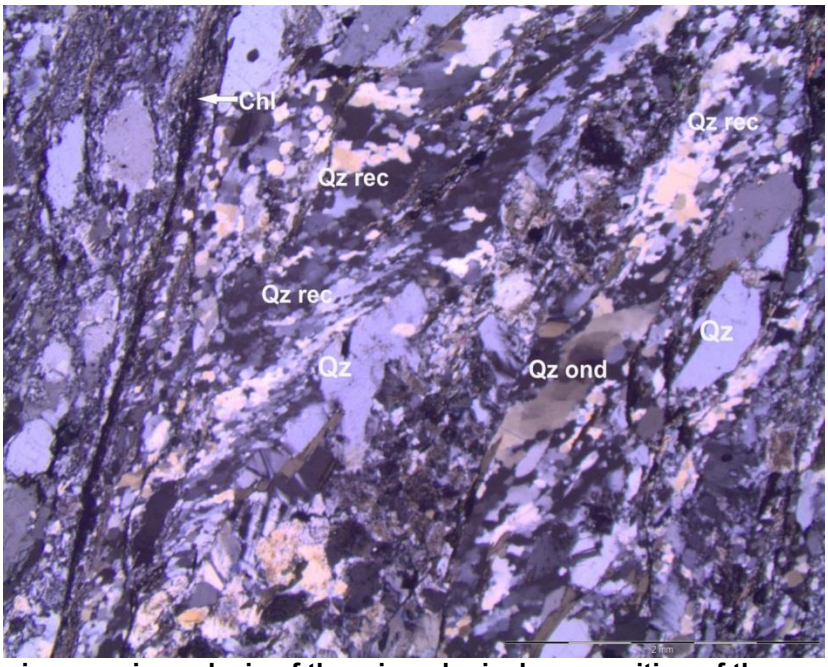

Figure 41: microscopic analysis of the mineralogical composition of the aggregate (Marins, 2021)

3.2.2 Tank and Heating System

The tank used in this study was a plastic tank (with a capacity of 100 liters), in which a heating system (Fig. 42) was mounted using reactors (Fig. 43), similar to those used in conventional heaters, coupled to a thermocirculator.

Figure 42: Tank with the heating system (Author, 2020)

Figure 43: Reactor used in the heating system
(Author, 2020)

In order to avoid loss of temperature to the environment, the tank has been thermally insulated. (Fig.44)

Figure 44: Thermal insulation of the tank
(Author, 2020)

3.2.3 Instrumentation: Sensors, Machines And Data Acquisition System

To measure the evolution of strains and stresses in concrete during the tests, fiber optic sensors, type FBG (Fiber Bragg Grating sensor). They are made of silica with a thin polyamide coating and Bragg reference wavelengths around 1550nm, which allows their interrogation by FS22. This type of sensor was chosen because the sensor is limited to the size of the optical fiber (Fig. 45) in addition it is a type of sensor extremely sensitive to the physical parameters whose evolution must be measured.

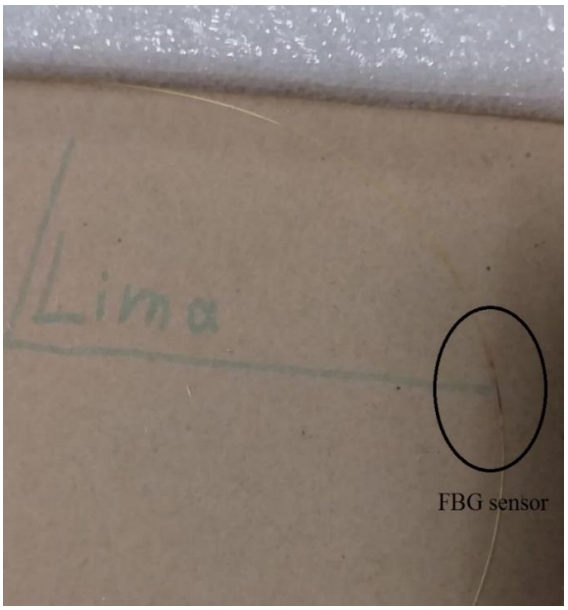

Figure 45: Fiber Bragg Grating sensor
(Author, 2020)

The acquisition of the wavelengths were performed with an optical interrogator HBM FS22 DI Industrial BraggMETER (Fig. 46).

Figure 46: HBM FS22 DI Industrial BraggMETER optical interrogator
(Author, 2020)

Temperature sensors (PT100) were used (Fig. 47) to determine the temperature inside the concrete in order to compensate for the thermal expansion effects of the material when calculating the deformations.

Figure 47: Temperature measurement system and temperature sensor (Author, 2020)

The software used to collect measurement data by fiber optics sensors was developed at ICAM and the purpose of this program is to allow the acquisition and saving of the Bragg wavelengths measured by the braggmeter HBM FS 22 DI. This computer program has a simplified and intuitive interface (Fig. 48)
and allows a measurement of wavelengths every 5 minutes, or with the desired time, in addition it is possible to receive simultaneous information from fibers connected in the four channels of the FS 22.

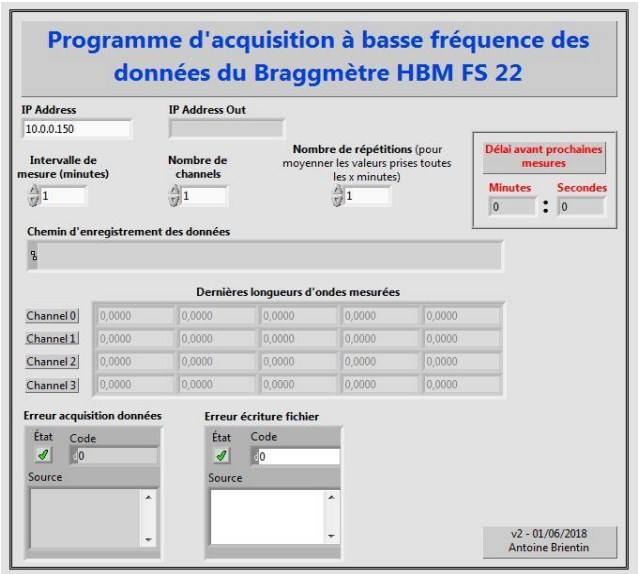

Figure 48: software for FBG measurements: interface (Author, 2020)

3.3 METHODOLOGY

This section presents the methodology of this work, which was developed according to the protocol described in item 3.1. Initially it is presented how the concrete dosage calculations were made and the amount of chemical solution required in the samples and in the storage tank, based on the parameters indicated by RILEM AAR-4 (2016).

After defining the proportions, it is shown how the concrete prisms were molded, in which sensors of the FBG type and PT100 sensors were inserted to obtain the deformation and temperature data. Finally, the calculation procedure used to obtain the results is presented.

3.3.1 Concrete Mix Design

Cement Content = 440 Kg/m^3 (Tab. 4)
Density of cement = 3.13 g/cm^3 (Tab. 1)
Na_2O eq = Na_2O% + 0.658Xk_2O% = 0.24% (Tab. 2)

Cement content	440 kg/m^3
Free (effective) water content	220 kg/m^3
Coarse aggregate	60 % by mass
Fine aggregate	40 % by mass
Air content	<3 %

Table 4 - General Concrete Mix Design (RILEM AAR-4, 2016)

3.3.1.1 Calculation of Proportions

Material	Grading (mm)	Proportion (%)	Quantity (kg/m^3)	Volume (L/m^3)
Coarse aggregate	4/16	60	X	X/2.68
Fine aggregate	0/4	40	4/6 × X	(4/6 × X)/2.68
Cement	–	–	440	(440/3.08) = 143
Water (free)	–	–	220	220

Table 5 – Concrete Mix Design (RILEM AAR-4, 2016)

- Coarse Aggregate (vol) = 60% → (600*1.379)/2.68 = 308.7 dm3
  (1.379 → Density)
- Coarse Aggregate (Mass) =308.7x2.68= 827.4 Kg/m^3
- Sand (vol) = 1000 – (140.6+220+308.7+30) = 300.7 dm3
  (1000 → 1m3; 30 → 3% of 1000 (air content))
- Sand (Mass) = 300.7x2.68 = 805.9 Kg/m^3

CEM	SAND	COARSE AG	W/C
440	805.9	827.4	220
1	1.83	1.88	0.5

Table 6 – Dosage
(Author, 2020)

3.3.1.2 Calculation of Sodium Hydroxide to be added to the Mixing Water

Calculation to determine the amount of sodium hydroxide (NaOH) to be added to the mixing water to increase the alkali content up to 1.25 % sodium oxide equivalent by mass of cement:

Cement content of 1 m^3 of concrete = 440 kg
Specified amount of Na2O eq in concrete = 440 x 0.0125 = 5.5 kg
Amount of Na2O eq in cement 0.24 %= 440 x 0.0024 kg = 1.056 kg
Amount of Na2O eq to be added per m^3 = 5.5 – 1.056 = 4.444 kg

The conversion factor Na2O eq to NaOH is 1.291

Amount of NaOH required to be added to the mixing water = 4.444 x 1.291 = 5.737 kg/m3

The prisms will be molded and placed in an alkaline solution and equivalent to the internal environment to prevent leaching.

Unit Volume (1 Prism) = 0.001603125 m^3
Total Volume (3 prisms) = 0.004809375 m^3

Total Vol = 0.00481 + 10% = 0.0053 m3

X_{NaOH}= 0.0304 kg

3.3.1.3 Calculation of Sodium Hydroxide to be added to the Tank Water

Capacity of the Tank: 100 L

Quantity required: 1.25% of NaOH

1.25% = 0.3125 N = 12.5 g/L

For 100L = 1.250 kg

3.3.2 Concrete Molding and Measurements

After defining the dosage required to make the concrete, molding was done. To ensure that the optical fiber was located in the middle of the concrete prism, an opening was left in the shape before molding (Fig. 49)

At the time of molding, the concrete was placed in half the shape, the fiber optic sensor was inserted and positioned at the average height of the concrete prism (Fig. 50). The temperature sensor was also inserted at that moment, away from the fiber optic sensor to avoid causing any type of interference (Fig. 51).

Figure 49: Molds with hole for sensor insertion
(Author, 2020)

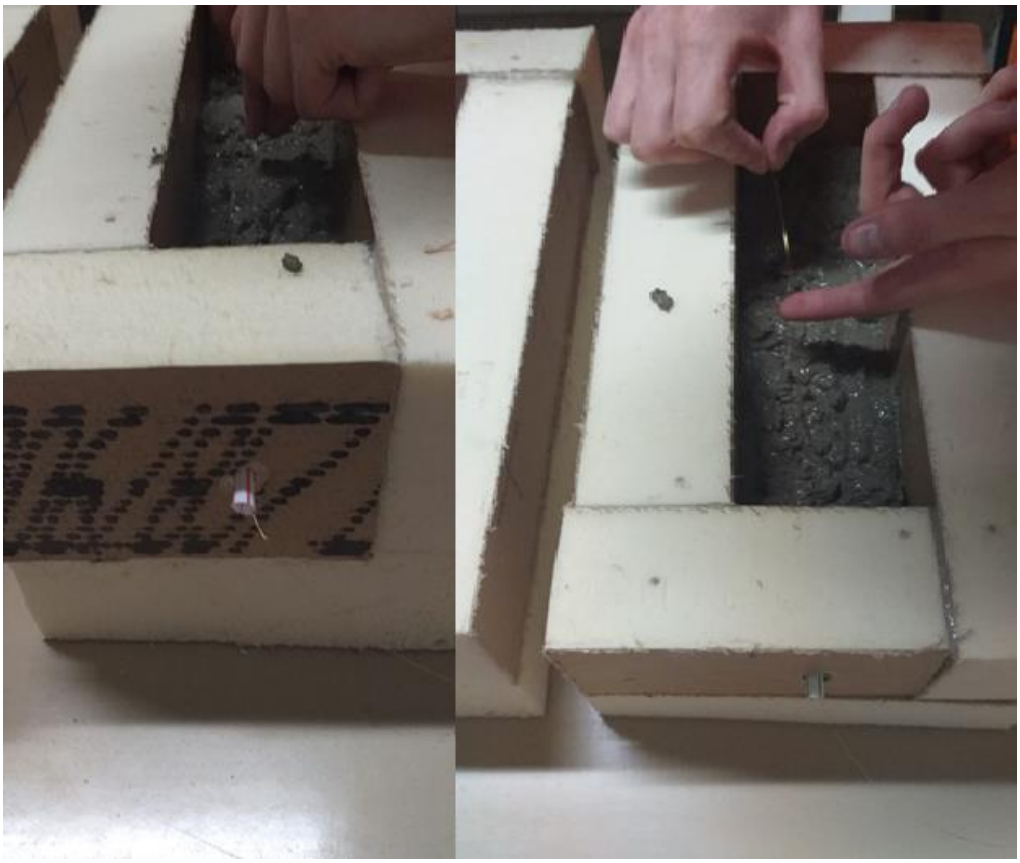

Figure 50: Fiber optic sensor insertion
(Author, 2020)

Figure 51: Temperature sensor insertion
(Author, 2020)

After the insertion of the sensors in the three prisms, the molding was finished with the second layer of concrete (Fig. 52). The measurements started to be made immediately after the molding of the prisms.

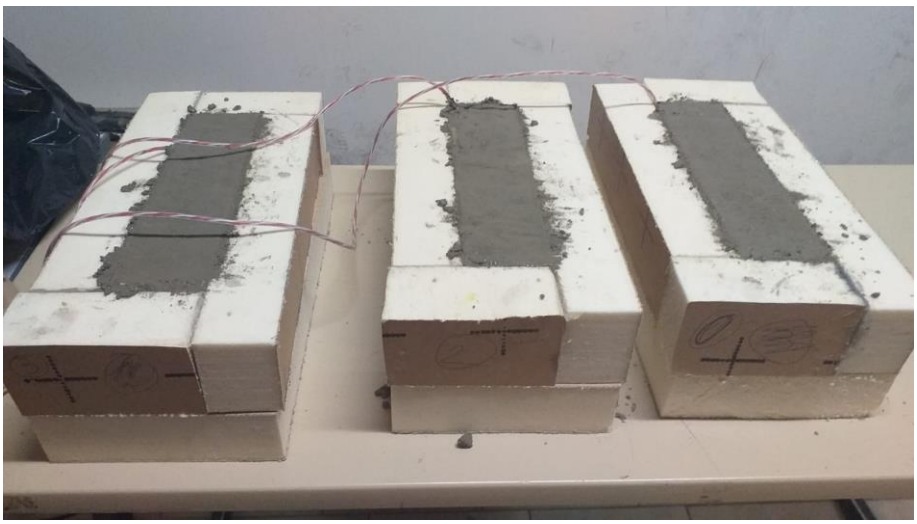

Figure 52: Prisms molding
(Author, 2020)

The shapes were made in a material that made it possible to unmold without any damage to the optical fiber. In this way it was possible to cut out the shapes to remove the concrete (Fig. 53).

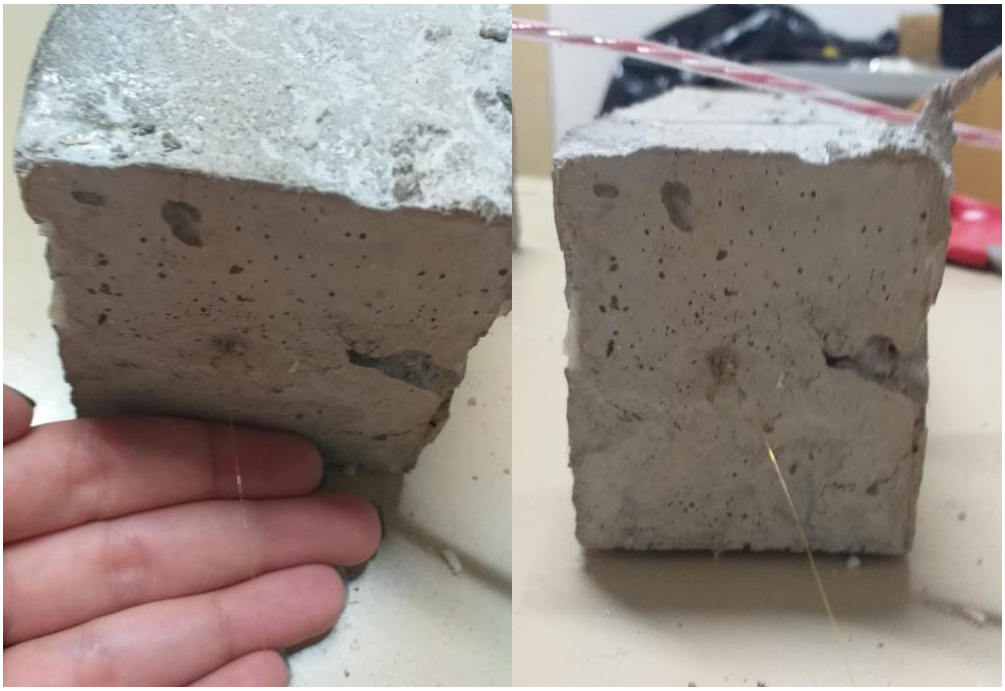

Figure 53: Concrete prisms after demoulding
(Author, 2020)

After demoulding, two of the prisms were placed in the tank (Fig. 54) with an alkaline solution of 1.25% NaOH. After placing the prisms in the tank, the thermocirculator was

turned on and the temperature gradually increased until stabilization at around 70 ° C, a temperature that remained constant during the tests.

Figure 54: Concrete prisms inside the tank
(Author, 2020)

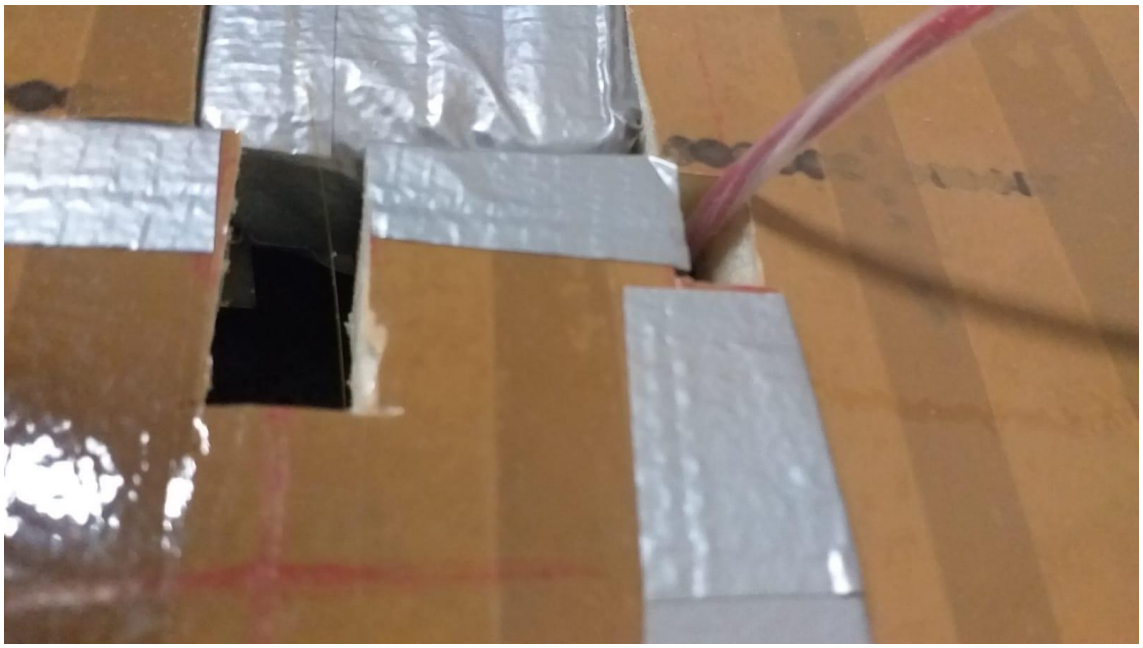

Figure 55: Openings to Allow the Passage of the Sensors
(Author, 2020)

During the tests, it was necessary to avoid the maximum possible loss of temperature to the environment, however, from the assembled system, it was necessary to maintain some openings (Fig. 55), such as the openings left in the tank cover for the sensors to pass. The temperature loss to the environment was around 10 ° C and to maintain the temperature of the alkaline solution around 70 ° C, the loss was compensated by increasing the temperature of the thermocirculator (Fig. 56).

Figure 56: Temperature variation between the machine and the NaOH solution (Author, 2020)

Measurements were started immediately after molding the concrete prisms and an interval of 5 minutes was defined between wavelength measurements. This time was defined so that, in case there was any damage or failure in the equipment's response, it was possible to know more precisely when the failure occurred. The sensors were identified according to the channel number from which the measurements came out (Tab. 7), in order to know which prism each sensor represented.

FBG	PT	CONDITION OF THE PRISM
CHANNEL 0	0	Inside NaOH solution
CHANNEL 2	2	Inside NaOH solution
CHANNEL 3	3	Normal conditions

Table 7 – sensors identification (Author, 2020)

3.3.3 Methodology for obtaining the results

To obtain the results, the output data of the software used were analyzed. Every 5 minutes, new FBG wavelength data was obtained by the program, as well as temperature information obtained by the PT100 sensor. With these data, it is possible to obtain information about the deformation of the material.

According the equation that gives the response of an FBG sensor, the total deformation is given by:

$$\varepsilon_{total} = (\Delta\lambda_{\text{Bragg}} / \lambda_{\text{Bragg ref}} - KT * \Delta T) * 1/K_{\varepsilon} \quad (7)$$

In this case, KT and Kε are fiber-dependent constants, being 7.8 x10^{-6} ° C and 0.78 x10^{-6} (μm / m) respectively.

ΔT corresponds to the temperature variation, always in relation to the reference measure and λ_{Bragg} are the wavelength readings provided by the measuring equipment.

Knowing that the cement hydration process in the concrete causes the release of heat, one cannot neglect the temperature variations in the material, which at this stage are quite significant, so is necessary to consider the thermal effects at the time of calculation.

Aiming to calculate the effects of material shrinkage, which should be used is as follows:

$$\varepsilon_{total} = \alpha_{\text{concrete}} * \Delta T + \varepsilon_{\text{shrinkage}} \Rightarrow \varepsilon_{\text{shrinkage}} = \varepsilon_{total} - \alpha_{\text{concrete}} * \Delta T \quad (8)$$

Where α_{concrete} is the coefficient of thermal expansion of concrete represented by 10x10^{-6} K^{-1}

4 RESULTS AND DISCUSSION

In this session, the results and discussions regarding the analyzes carried out in the experimental program are presented. First, the results obtained through the readings performed by the FBG sensor in the prism maintained under normal environmental conditions are discussed, then the results related to the use of FBG sensors placed on the prisms subjected to the aggressive environment are discussed to induce the occurrence of internal swelling reactions.

4.1 FBG SENSORS IN CONCRETE MAINTAINED UNDER NORMAL ENVIRONMENTAL CONDITIONS

As previously mentioned, the measurements were started immediately after molding the prisms and the measurements were taken every 5 minutes as defined as *input* in the software. The optical fibers used in this work had 5 sensors of the FBG type along their length, however only 1 (FBG 5) was located inside the concrete prisms, due to the dimensions of the prisms and the distance between the sensors was not possible to place more than one inside the concrete.

Figure 57 shows the table used to obtain the data. The table was updated daily with the wavelength information provided by the software and the deformation parameters we intended to obtain were calculated from the formulas described in item 3.3.3 (presented in the last two columns of the table).

id	Channel 3	date	Time	fbg 1	fbg 2	fbg 3	fbg 4	fbg 5	temp	Δλ (test-ref)	ΔT (test-ref)	Δλ/λref	Δε1	Δε2 (correct)	eshrinkage
1	Channel 3	31/08/2020	13:34:28	1542,9924	1551,0215	1558,7794	1567,0093	1574,9635	21,92	0,002386842	0,070526316	1,5155E-06	1,9429394	1,23767623	0,532413072
2	Channel 3	31/08/2020	13:50:08	1542,9927	1551,0213	1558,7806	1567,0106	1574,9636	21,79	0,002436842	-0,059473684	1,5472E-06	1,9836404	2,578377275	3,173114117
3	Channel 3	31/08/2020	14:05:48	1542,9963	1551,0366	1558,8123	1567,0331	1575,0479	24,63	0,086786842	2,780526316	5,5104E-05	70,646304	42,84104122	15,03577806
4	Channel 3	31/08/2020	14:20:31	1542,9934	1551,0291	1558,7799	1567,0692	1575,0587	24,61	0,097586842	2,760526316	6,1961E-05	79,43773	51,83246707	24,22720392
5	Channel 3	31/08/2020	14:26:11	1542,9958	1551,0316	1558,7839	1567,0652	1575,0566	24,47	0,095486842	2,620526316	6,0628E-05	77,728286	51,52302316	25,31776
6	Channel 3	31/08/2020	14:31:51	1542,9947	1551,0297	1558,7817	1567,0688	1575,0568	24,37	0,095636842	2,520526316	6,0723E-05	77,850389	52,64512629	27,43986314
7	Channel 3	31/08/2020	14:37:31	1542,9932	1551,0296	1558,7813	1567,0684	1575,0551	24,31	0,093936842	2,460526316	5,9644E-05	76,466554	51,86129074	27,25602759
8	Channel 3	31/08/2020	14:43:11	1542,9935	1551,0303	1558,7813	1567,0681	1575,0533	24,29	0,092136842	2,440526316	5,8501E-05	75,001316	50,5960531	26,19078994
9	Channel 3	31/08/2020	14:48:51	1542,9945	1551,0316	1558,7805	1567,0716	1575,0539	24,27	0,092386842	2,420526316	5,866E-05	75,204821	50,99955833	26,79429517
10	Channel 3	31/08/2020	14:54:31	1542,993	1551,0306	1558,7807	1567,072	1575,052	24,23	0,090836842	2,380526316	5,7676E-05	73,943089	50,13782592	26,33256276
11	Channel 3	31/08/2020	15:00:11	1542,9923	1551,0285	1558,7881	1567,0744	1575,0519	24,22	0,090736842	2,370526316	5,7612E-05	73,861687	50,15642382	26,45116067
12	Channel 3	31/08/2020	15:05:51	1542,9922	1551,0294	1558,7877	1567,0734	1575,0522	24,2	0,091036842	2,350526316	5,7803E-05	74,105893	50,6006301	27,09536694
13	Channel 3	31/08/2020	15:11:31	1542,9921	1551,0284	1558,7878	1567,0717	1575,0521	24,2	0,090936842	2,350526316	5,7739E-05	74,024491	50,51922801	27,01396485
14	Channel 3	31/08/2020	15:17:11	1542,9912	1551,028	1558,7871	1567,0707	1575,0519	24,21	0,090786842	2,360526316	5,7644E-05	73,902388	50,29712487	26,69186171
15	Channel 3	31/08/2020	15:22:51	1542,9914	1551,028	1558,7869	1567,0701	1575,0521	24,2	0,090936842	2,350526316	5,7739E-05	74,024491	50,51922801	27,01396485
16	Channel 3	31/08/2020	15:28:31	1542,9915	1551,027	1558,7869	1567,0692	1575,0524	24,23	0,091286842	2,380526316	5,7961E-05	74,309398	50,50413533	26,69887217
17	Channel 3	31/08/2020	15:34:11	1542,9914	1551,0278	1558,7868	1567,0699	1575,0538	24,26	0,092686842	2,410526316	5,885E-05	75,449028	51,3437646	27,23850145
18	Channel 3	31/08/2020	15:39:51	1542,9907	1551,0266	1558,7866	1567,0699	1575,0548	24,29	0,093686842	2,440526316	5,9485E-05	76,263049	51,85778552	27,45252236
19	Channel 3	31/08/2020	15:45:31	1542,9906	1551,0274	1558,7864	1567,0706	1575,0573	24,32	0,096136842	2,470526316	6,1041E-05	78,2574	53,55213675	28,84687359
20	Channel 3	31/08/2020	15:51:11	1542,9908	1551,0265	1558,7872	1567,0711	1575,06	24,36	0,098836842	2,510526316	6,2755E-05	80,455256	55,34999321	30,24473006
21	Channel 3	31/08/2020	15:56:51	1542,9913	1551,0265	1558,7862	1567,0712	1575,0622	24,42	0,101086842	2,570526316	6,4184E-05	82,286803	56,58154027	30,87627711
22	Channel 3	31/08/2020	16:02:31	1542,9903	1551,0264	1558,786	1567,0713	1575,0662	24,47	0,105036842	2,620526316	6,6692E-05	85,502186	59,29692287	33,09165971
23	Channel 3	31/08/2020	16:08:11	1542,9904	1551,0265	1558,7854	1567,0718	1575,0711	24,57	0,109936842	2,720526316	6,9803E-05	89,490888	62,28562534	35,08036218
24	Channel 3	31/08/2020	16:13:51	1542,99	1551,0266	1558,7853	1567,0712	1575,0768	24,64	0,115636842	2,790526316	7,3422E-05	94,130808	66,22554454	38,32028138
25	Channel 3	31/08/2020	16:19:31	1542,9905	1551,0262	1558,7861	1567,0713	1575,0823	24,76	0,121186842	2,910526316	7,6946E-05	98,648624	69,5433606	40,43809744
26	Channel 3	31/08/2020	16:25:11	1542,9896	1551,0261	1558,7861	1567,0724	1575,0879	24,89	0,126736842	3,040526316	8,047E-05	103,16644	72,76117666	42,35591351
27	Channel 3	31/08/2020	16:30:51	1542,9902	1551,0263	1558,7849	1567,0714	1575,0952	25	0,134036842	3,150526316	8,5105E-05	109,10879	77,60352932	46,09826617

Figure 57: Data obtained in the tests
(Author, 2020)

For this prism, due to the conditions in which the material was subjected, it was possible to calculate the effects of the shrinkage using the equation 8 (shown previously). The graph in figure 58 presents the measurements of deformation (FBG 5) and temperature (PT100) and shrinkage of the concrete that remained at normal temperature and environmental conditions.

The Shrinkage results ($\varepsilon_{shrinkage}$) represented by the yellow line, wich presents a behavior compatible with the expected, showing negative deformations, because the loss of moisture to the environment promotes material shortening.

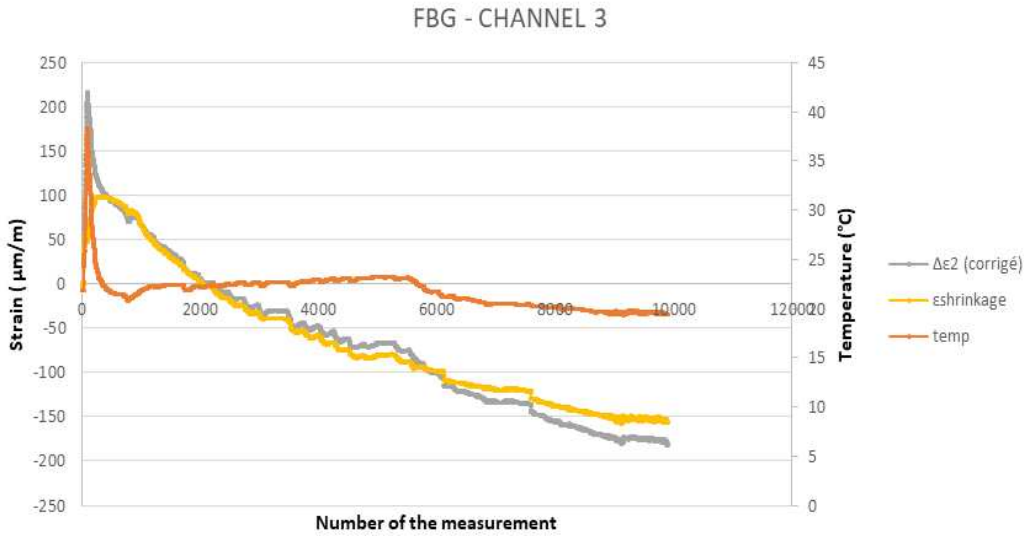

Figure 58: Measurements FBG Channel 3
(Author, 2020)

Figures 59 and 60 show the maximum deformation and temperature points, which occurred at the beginning of the process, which was also expected, due to the cement hydration process being an exothermic process. These points of the graph reaffirm the sensitivity of the FBG sensor used, which continuously detected the wavelength variations coming from the deformation processes of the material.

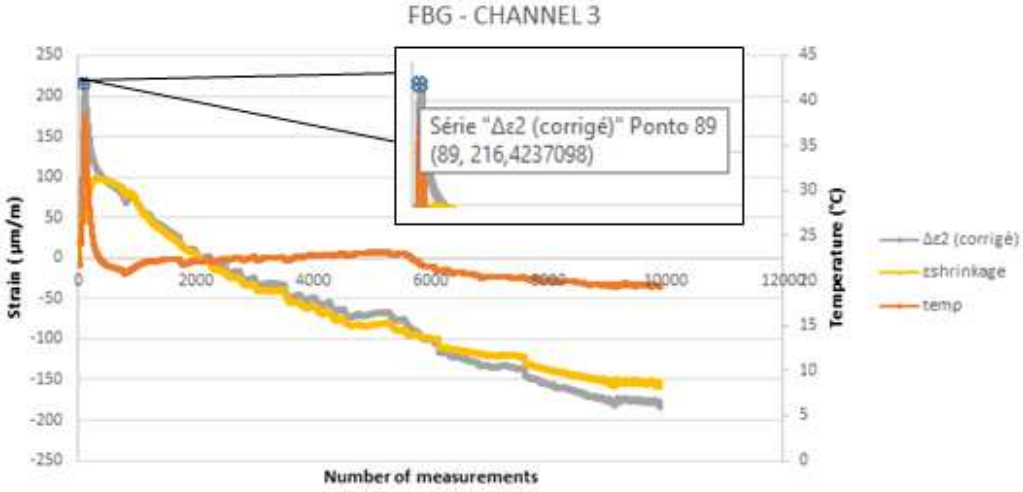

Figure 59: Maximum deformation point
(Author, 2020)

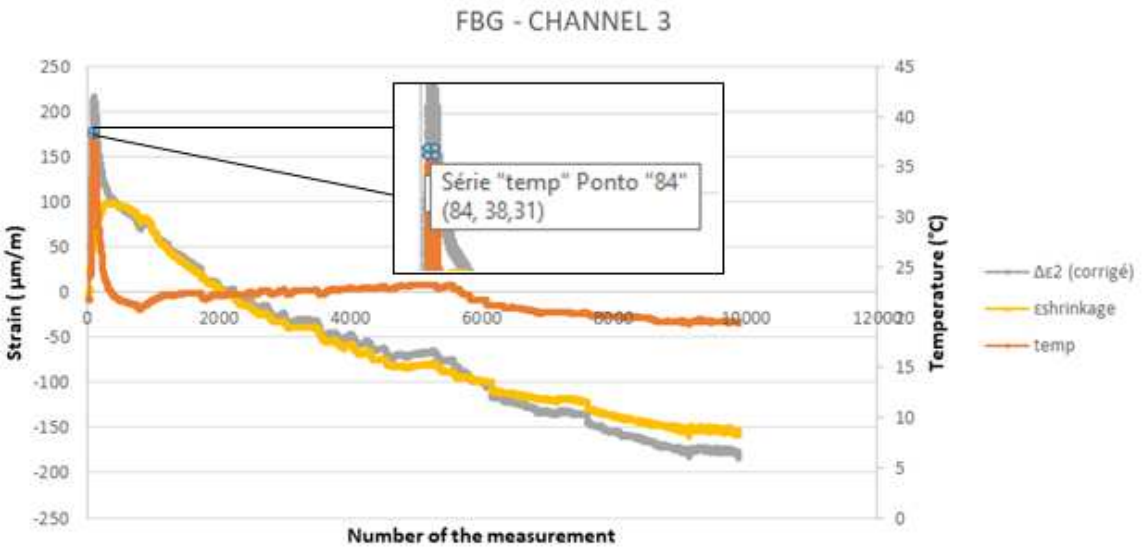

Figure 60: Maximum temperature point
(Author, 2020)

It was observed through the data table used to obtain the results that the readings of the 28th day after the concrete molding occurred from the measurement of number 7000. The Figure 61 shows the shrinkage measurement point of the concrete used at 28 days. The result is satisfactory and compatible with the results commonly presented by the literature.

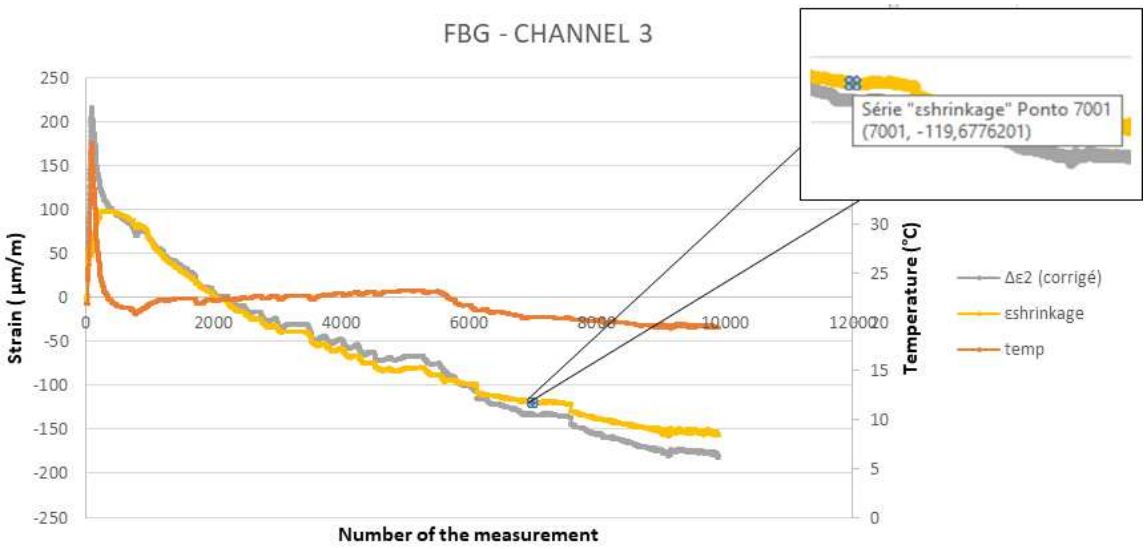

Figure 61: Shrinkage at 28 days after molding
(Author, 2020)

We can observe that, the continuous reading of the parameters presented, make possible a good monitoring of the material, and allows the consultation of the data at any age within the period in which the readings were taken.

After 40 days of continuous readings, (which resulted in approximately 10000 readings) the sensor, which was located inside the prism that was kept under normal environmental conditions, started to fail in the measurements. The FS22 DI BraggMETER has in its configuration the minimum optical power defined, if the sensor response is below the minimum value, it is not possible to obtain the measurement results.

Figures 62 and 63 represent (respectively) the optical fiber with the sensors working normally and the optical fiber with 4 sensors operating and 1 (exactly the sensor located inside the concrete) with weak response (below the minimum optical power), which made continuity measurements impossible.

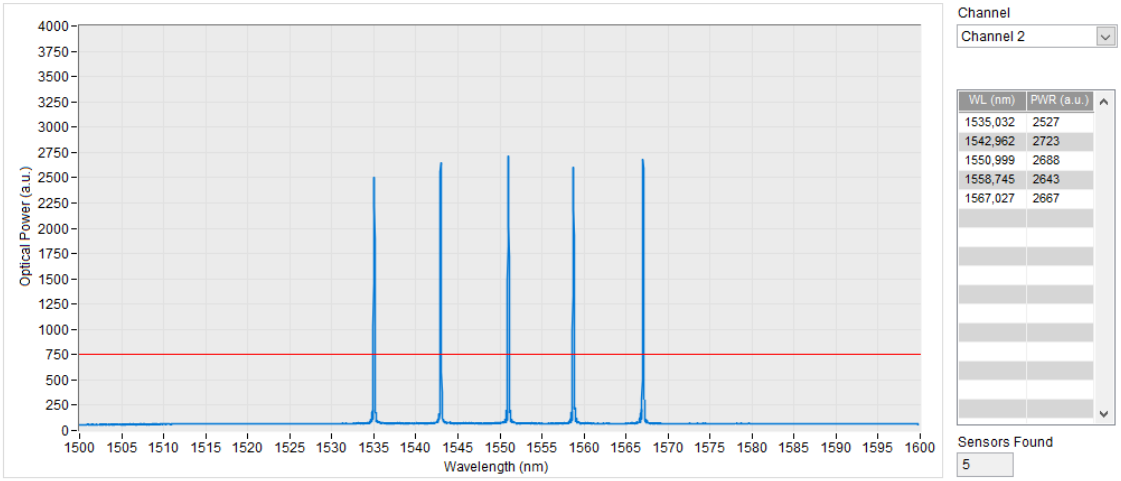

Figure 62: Fiber optic sensors working normally
(Author, 2020)

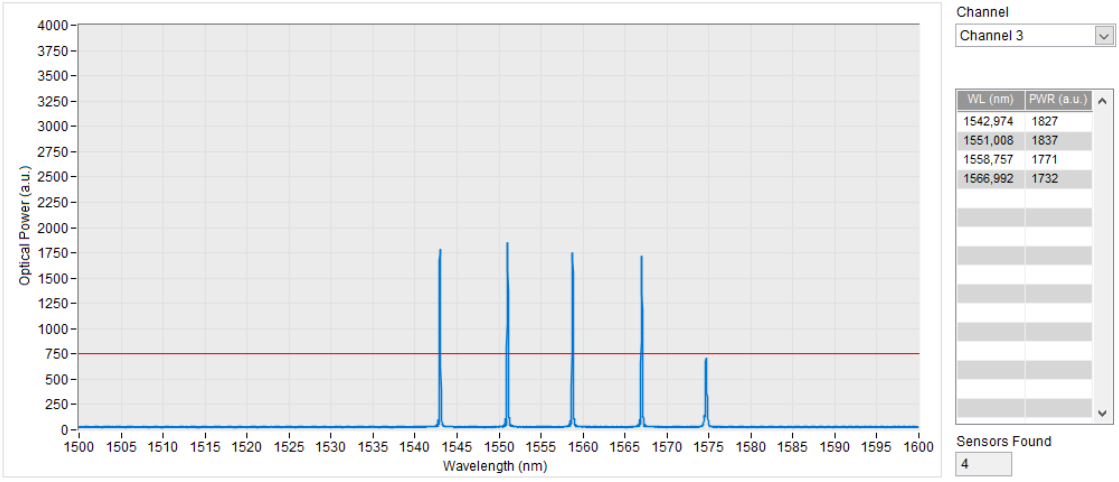

Figure 63: Fiber optic sensor inside the prism without working correctly after 40 days of measurements
(Author, 2020)

In this case, what may have caused the measurement failures is the material itself, as it is known that the concrete itself is an alkaline medium, and this concrete in particular had 1.25% alkali in its composition. The alkalis in the concrete may have reacted with

the fiber material (slowly, since it was at room temperature) causing some damage and making it impossible to proceed with the measurements.

4.2 FBG SENSORS IN CONCRETE PLACED IN AN AGGRESSIVE ENVIRONMENT

Regarding the prisms that were placed in an aggressive environment (channel 0 and channel 2) in order to accelerate the alkalis-aggregate reaction, the graphs presented in figures 64 and 65, show the total deformations in each prism (measurements obtained through the readings of the FBG sensors applied to equation 7 and also the temperature measured by the PT100 sensors in the same time interval).

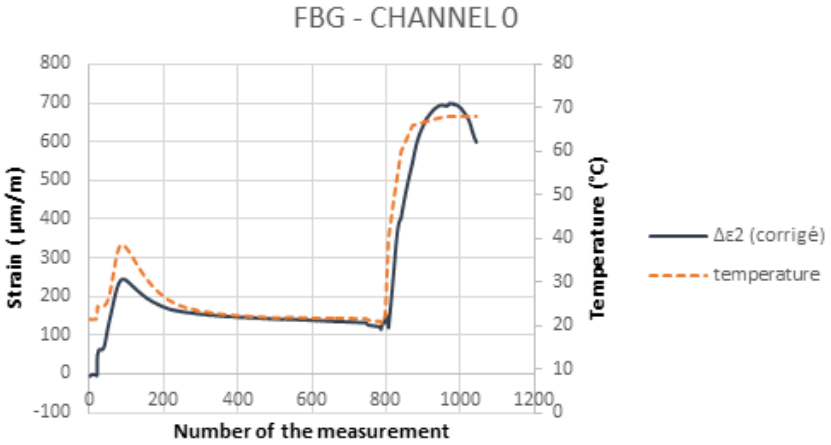

Figure 64: Measurements FBG Channel 0
(Author, 2020)

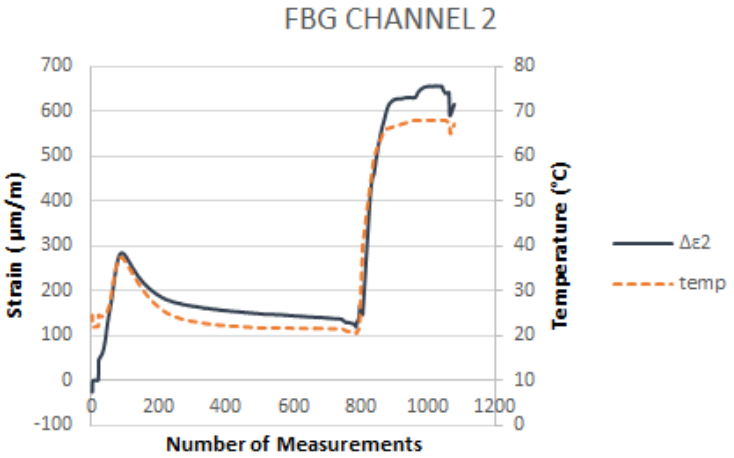

Figure 65: Measurements FBG Channel 2
(Author, 2020)

in figure 66 it is possible to observe that the prisms showed similar behavior in the first hours after molding, where there is a peak in temperature and deformation, a behavior

that was seen previously in the first results presented and which is consistent with the expected.

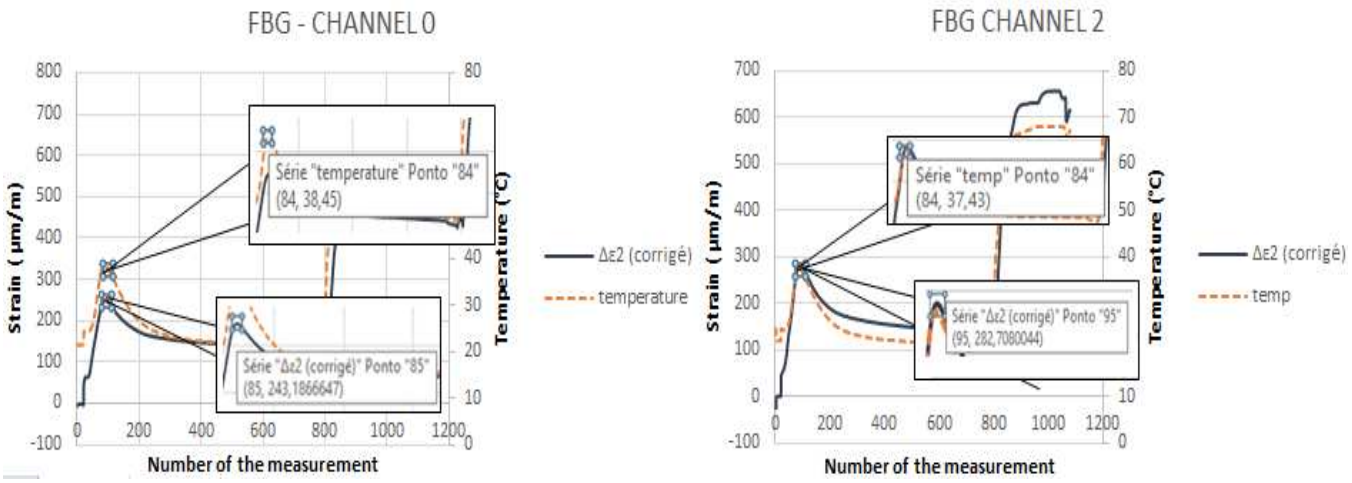

Figure 66: Comparing the behavior of the prisms in the first hours (Author, 2020)

Considering the three prisms used in the tests, table 8 shows that in the first hours the maximum values found for deformation and temperature are very similar and have the same order of magnitude, which represents a good functioning of the sensors and consistent results.

MAXIMUM MEASURES (FIRST HOURS AFTER MOLDING)		
CHANNEL	TEMP (°C)	STRAIN (µm/m)
CHANNEL 0	38,31	243,18
CHANNEL 2	38,45	282,7
CHANNEL 3	37,43	216,42

Table 8 – Maximum values found for deformation and temperature (Author, 2020)

In figures 64 and 65 and in the figure 67 also, it is possible to observe that from reading number 800 there is a considerable change in the graph curves, this is because this was the exact moment when the prisms were inserted in the NaOH solution with temperature growing gradually to 70 ° C.

The second peak of temperature and strain observed refers (Fig. 67) to the moment when the prisms were placed in the NaOH solution and subjected to high temperatures to accelerate internal swelling reactions. Figure 67 shows the maximum deformation and temperature points reached in the two prisms, before the sensors fail. It is noted that the behavior is very similar, which was already expected knowing that the prisms were subject to the same conditions.

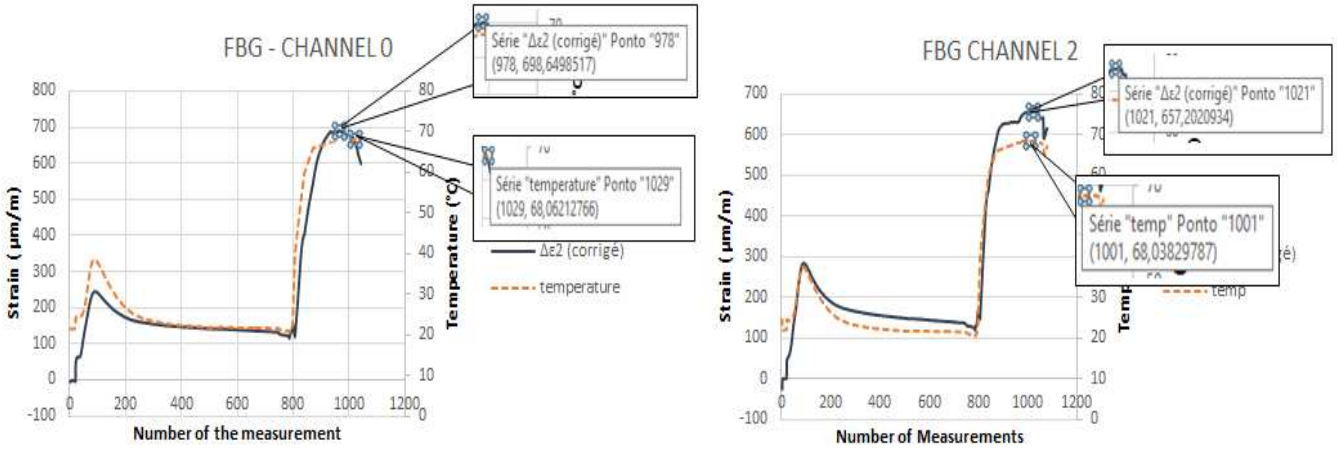

Figure 67: Comparison of prism behavior before sensor failure (Author, 2020)

It was desired to keep the measurements for at least 3 months, with the purpose of obtaining the appearance of some internal reaction of expansion and to measure the expansion related to that reaction (in this case the AAR) but it was observed that after one day of the prisms of concrete immersed in alkaline solution at 70 ° C, the sensors of both prisms stopped responding to the optical signals emitted by BraggMeter with only a few hours difference.

The loss of responses to optical signals can have several origins, and can even have more than one at the same time. The main hypotheses are as follows:

- The stress caused to the prism by the temperature may have caused internal cracks that interfered with the reception and re-emission of the signal;
- The thermal expansion of the concrete may have created a failure of the material to adhere with the optical fiber, causing a detachment for example and damaging the optical fiber;
- The use of exposed optical fiber (without cable), although it provided good adhesion of the fiber to the concrete, may have caused the loss of the signal at the beginning of the tests, because although the fiber withstands the temperature well, the behavior of the fiber material when associated temperature and NaOH solution was not known.

The first two hypotheses could not be specified, considering that it was not possible to remove the entire fiber from the concrete without damaging it, it was decided to microscopically analyze the part of the fiber that was in contact with the alkaline solution at 70 ° C at the top of the prisms. After the analysis, a considerable section loss (Fig. 68 and Fig. 69) was found in relation to the part of the fiber that was not in contact with the NaOH solution (with only one day of exposure of the material to the solution).

Figure 68: Optical fiber without contact with the NaOH solution
(Author, 2020)

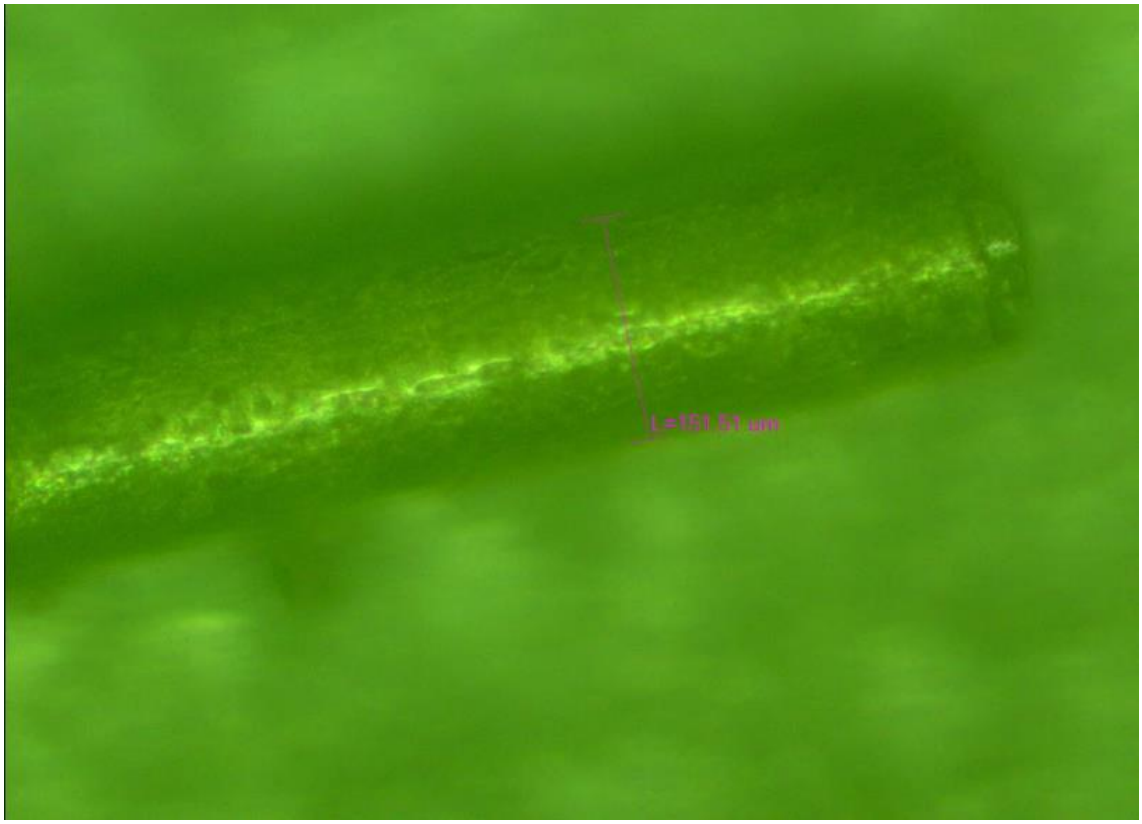

Figure 69: Optical fiber that was in contact with the NaOH solution
(Author, 2020)

The results of the microscopic analysis suggest that there was a reaction between the constituent materials of the fiber (polyamide and silica) with sodium hydroxide, a reaction potentiated by the elevated temperature. These damages found in the fiber may have caused the loss of optical responses prematurely.

It is extremely important to say that, due to the pandemic context in which this work was developed, it was not possible to test other types of fibers or sensors in a feasible time, as was intended. There was a difficulty in performing experimental tests in the laboratory due to the isolation measures practiced around the world, a fact that prevented laboratory practices in most universities in the world.

5 CONCLUSIONS

From this work it can be concluded that new technologies have often been implemented as promising resources in the analysis of structures and materials used in civil engineering.

According to the literature, it is possible to perform measurements of several parameters through optical fiber sensors, being more used for measurements of deformations of the material when subjected to the most diverse conditions (loads, temperatures and deformations from shrinkage and internal swelling reactions)

From the tests carried out in this work, it was concluded that the fiber optic sensors of the FBG type are sensitive to small deformations and are useful for measurements of concrete deformations, however, the design of the optical fiber used, although it has presented a good adhesion with concrete, it is not the most suitable for this type of analysis.

The deformation measurements that were possible, including the measurement of shrinkage of the concrete maintained under normal environmental conditions, proved to be compatible with the literature, but it was not possible to continue due to failures in the reception and re-emission of optical signals by the sensors. Although the sensor has stopped receiving optical signals due to deterioration of the optical fiber, it is important to note that it has been possible to perform a series of continuous readings of more than 10,000 measurements, which is a high number of measurements and that no other method of measurement deformation assessment of concrete can currently perform so quickly and accurately.

The work aimed to evaluate the possibility of measuring expansions due to internal expansion reactions, for this purpose, due to the test conditions and the type of fiber used, the sensor was not efficient in terms of durability.

For measurements in a short period and under normal conditions, this design may be appropriate, but in the long run it has not proved efficient. For laboratory tests that require different conditions, as well as for work carried out on real structures, the most appropriate is the use of optical fibers protected by reinforced cables, where the fiber and the sensor are not in direct contact with the material but still be sensitive enough to measure small deformations (if this is the purpose of use).

REFERENCES

AHMED, T; BURLEY, E.; RIGDEN, S. and ABU-TAIR, A.I., **The Effect of Alkali Reactivity on the Mechanical Properties of Concrete**. Construction and Building Materials Vol. 14 2003.

ALLENA, S. **State-of-the-Art Review on Early-Age Shrinkage of Concrete.** The Indian Concrete Journal. 85. 14-20, 2011.

ALMEIDA, T. S. **Synthesis and characterization of gels of the alkali-silica reaction in accelerated conditions**, doctoral thesis, federal university of Paraíba, 2015. (in portuguese)

BAO, T., WANG, J., & YAO, Y. **A fiber optic sensor for detecting and monitoring cracks in concrete structures.** Science China Technological Sciences, 2010

BARRIAS, A., CASAS, J., & VILLALBA, S. **Embedded Distributed Optical Fiber Sensors in Reinforced Concrete Structures - A Case Study**. Sensors, 18, 2018.

BAZANT, Z. P. **Creep and shrinkage prediction model for analysis and design of concrete structures: Model B3.** Adam Neville Symposium: Creep and Shrinkage - Structural Design Effects ACI SP-194, (pp. 1-83). Farmington, Michigan, 2000.

BAZANT ZP, WITTMANN FH, EDITORS. **Creep And Shrinkage In Concrete Structures**. New York: Wiley; 1982

BAŽANT Z. P., JIRÁSEK M. **Creep and Hygrothermal Effects in Concrete Structures** Springer Netherland, 2018

BOUZABATA, H., MULTON, S., SELLIER, A., & HOUARI, H. **Swellings due to alkali-silica reaction and delayed ettringite formation: Characterisation of expansion isotropy and effect of moisture conditions.** Cement and Concrete Composites, 34, 2012.

BROOKS, J. J. **Influence of slag type and replacement level on strength, elasticity, shrinkage, and creep of concrete.** ACI Proceedings Fourth International Conference: Fly Ash, Silica Fume, Slag, and Natural Pozzolans in Concrete, Vol. 2, pp. 1325-1341. Istanbul, Turkey, 1992.

BROOKS, J. J. **Dimensional stability and cracking processes in concrete.** Durability of Concrete and Cement Composites, 45–85, 2007.

BROWN, P.W., BOTHE, J.V. **The stability of ettringite.** Advances in Cement Research, 1993.

BRUNETAUD, X., DIVET, L., & DAMIDOT, D. **Impact of unrestrained Delayed Ettringite Formation-induced expansion on concrete mechanical properties.** Cement and Concrete Research, 38(11), 2008.

CASTRELLON-URIBE, J. **Optical Fiber Sensors: An Overview**. Fiber Optic Sensors, Chapter 1, 2012

CHATTERJI, S. **Mechanisms of alkali-silica reaction and expansion.** Proceedings of the 8th International Conference of the Alkali-Aggregate Reaction in Concrete, Kyoto, 1989.

COLLEPARDI, M., **A state-of-the-art review on delayed ettringite attack on concrete.** Cement and Concrete Composites, 25, 2003.

DAY, R., & CLARKE, J. **Plastic and thermal cracking.** Advanced Concrete Technology, 3–17, 2003.

DENG, L. & CAI, C. S., **Applications of fiber optic sensors in civil engineering**. Structural Engineering and Mechanics, vol. 25, no. 5, Mar. 2007

DESCHENES D. J., BAYRAK, O., FOLLIARD K. J., **ASR/DEF-damaged bentcaps: shear tests andfield implications.** Technical Report, Texas Department of Transportation. 2009.

DHIR, R. K., DE BRITO, J., SILVA, R. V., & LYE, C. Q. **Deformation of Concrete Containing Recycled Concrete Aggregate.** Sustainable Construction Materials, 2019.

DIVET, L. **Les réactions sulfatiques internes au béton: contribution à l'étude des mécanismes de la formation différée de l'ettringite**. Etudes et recherches des laboratoires des Ponts et Chaussées, 40, 2001.

DUNANT, C.F.; SCRIVENER, K.L. **Effects of uniaxial stress on alkali–silica reaction induced expansion of concrete**. Cement and Concrete Research, 42(3), 567–576, 2012

FERRARIS, C. F. **Alkali-Silica Reaction and High Performance Concrete.** Report NISTIR 5742. National Institute of Standards and Technology, Building and Fire Research Laboratory, Gaithersburg, Maryland, 1995.

FOURNIER B, BÉRUBÉ, M. A., FOLLIARD, K. J. and THOMAS, M. D. A**. Report on the Diagnosis, Prognosis, and Mitigation of Alkali-Silica Reaction (ASR) in Transportation Structures.** Federal Highway Administration, 2010.

FOURNIER B., BÉRUBÉ, M. A. **Alkali-aggregate reaction in concrete: a review of basic concepts and engineering implications**. Can J Civ Eng. 27, 2000.

GIACCIO, G., ZERBINO, R., PONCE, J., and BATIC, O. **Mechanical behavior of concretes damaged by alkali-silica reaction.** Cement and Concrete Research 38, 2008.

GILLOTT, J.E. **Alkali-reactivity problems with emphasis on Canadian aggregates.** Engineering geology. v. 23, 1986.

GODART, B, DIVET, L. **Lessons learned from structures damaged by delayed ettringite formation and the French prevention strategy.** Fifth international conference on Forensic Engineering, Institution of Civil Engineers, 2013

GODART, B. **Pathology, assessment and treatment of structures affected by Delayed Ettringite Formation**. Structural engineering international, 27 (3), 2017

GRATTAN, K. T. V., SUN, T. **Fiber Optic Sensor Technology: Introduction and Overview** - Optical Fiber Sensor Technology**:** Fundamentals, chapter 1, Springer Science+Business Media, 2000.

HISHAM K. H. **Optical Fiber Sensing Technology: Basics, Classifications and Applications.** American Journal of Remote Sensing. Vol. 6, No. 1, 2018

ICENHOWER, J. P., & DOVE, P. M., **The dissolution kinetics of amorphous silica into sodium chloride solutions: effects of temperature and ionic strength**. Geochimica et Cosmochimica Acta, 64(24), 2000

INGHAM, J. **Briefing: Delayed ettringite formation in concrete structures.** Proceedings of the Institution of Civil Engineers - Forensic Engineering, 165(2), 2012

JURCUT, A. C., **Modelling of alkali-aggregate reaction effects in reinforced concrete structures.** Thesis of master of applied science. Civil Engineering, University Toronto, 2015

KARTHIK, M. M., MANDER, J. B. HURLEBAUS, S. **ASR/DEF Related expansion in structuralconcrete: model development and validation.** Conctruction and building materials 128, 2016

KATAYAMA, T**. Late-expansive ASR in a 30-year old PC structure in eastern Japan**, Proc. 14th International Conference on Alkali–Aggregate Reaction (ICAAR), Austin, Texas, USA, 2012

KHAYAT, K. H. **Self-consolidating concrete for precast, prestressed concrete bridge elements.** Transportation Research Board of the National Academies, 2009.

KESAVAN, K., RAVISANKAR, K. PARIVALLAL, S. SREESHYLAM, P. SRIDHAR S. **Experimental studies on fiber optic sensors embedded in concrete,** Measurement, Vol. 43, 2010

KIHARA, Y. **Alkali-to-gregated reaction: mineralogical aspects.** In: 1st NATIONAL AGGREGATES SYMPOSIUM, São Paulo. USP, 1986. (in Portuguese)

KOVLER, K., AND ZHUTOVSKY, S., overview and future trends of shrinkage research, materials and structures, 2006, v. 39, pp. 827-847

LARIVE, C. **Apports combinés de l'expérimentation et de la modélisation à la compréhension de l'alcali-réaction et de ses effets mécaniques.** Thèse de doctorat, Ecole Nationale des Ponts et Chaussées, 1997.

LAU, K.T. **Fibre-optic sensors and smart composites for concrete applications**, Magazine of Concrete Research, 55, No. 1, 2003.

LEEMANN, KATAYAMA, FERNANDES and BROEKMANS, **Types of alkali–aggregate reactions and the products formed**. Proceedings of the Institution of Civil Engineers - Construction Materials – ICE, 2016.

LEGER, P., COTE, P., & TINAWI, R. **Finite element analysis of concrete swelling due to alkali-aggregate reactions in dams**. Computers & Structures, 60(4), 1996.

LEUNG, C. K. Y. **Fiber optic sensors in concrete: the future?** NDT&E International 34, 2001.

LEUNG, C. K. Y., WAN, K. T., JIANG, Y., **A Fiber Optic Sensor for Cracks in Concrete Structures**, Fracture Mechanics of Concrete Structures, Vol.2, edited by V.C. Li, C.K.Y. Leung, K. Willam and S. Billington, Conference paper, 2004.

Li, H.-N., Li, D.-S., and Song, G.-B. **Recent applications of fiber optic sensors to health monitoring in civil engineering.** Engineering Structures, 26, 2004

LUBEJ, S., ANZEL, I., JELUSIC, P., KOSEC, L., & IVANIC, A., **The effect of delayed ettringite formation on fine grained aerated concrete mechanical properties.** Science and Engineering of Composite Materials, 2014.

MAHDIKHANI, M. & BAYATI, Z. **Application and Development of Fiber Optic Sensors in Civil Engineering.** Beijing, China: The 14th World Conference on Earthquake Engineering, 2008.

MARINS, J. F. **Análise comparativa das normas NBR 15577:2018, AASHTO T 380:2018 e RILEM AAR-4.1:2016 para caracterização da reatividade de agregados graúdos utilizados na fabricação de concreto.** 2021. Dissertação (mestrado em engenharia) Programa de Pós Graduação em Engenharia Civil, Universidade Católica de Pernambuco, Recife, Brasil. (IN PROGRESS)

MARTIN, R. P., BAZIN, C., TOUTLEMONDE, F., **Alkali aggregate reaction and delayed ettringite formation: common features and differences**. 14th International conference on alkali aggregate reaction ICAAR14, 2012.

MARTIN, R. P., OMIKRINE-METALSSI, O., TOUTLEMONDE, F. **Modelling of concrete structures affected by internal swelling reactions : couplings between transfer properties, alkali leachning and expansion.** 2nd International conference on microstructure related durability of cementitious composites, France, 2012.

MEGGITT, B.T., **Fiber Optics in Sensor Instrumentation** - Chapter 17 in Instrumentation Reference Book (Fourth Edition), 2010.

MENDEZ, A., MORSE, T. F., MENDEZ, F. **Applications of Embedded Optical Fiber Sensors in Reinforced Concrete Buildings and Structures**. Fiber Optic Smart Structures and Skins II, 1990.

MERZBACHER C. I., KERSEY A. D., FRIEBELE, E. J. **Fiber optic sensors in concrete structures: a review.** In: Grattan K.T.V., Meggitt B.T. (eds) Optical Fiber Sensor Technology. Optoelectronics, Imaging and Sensing Series, vol 3. Springer, 1999.

MEHTA, P. K.; MONTEIRO, P. J. M. **Concreto: estrutura, propriedades e materiais**. 2ª ed. Reviewers: Nicole P. Hasparyk, Paulo Helene & Vladimir A. Paulon, Translate of the 4th edition in English with the title - Concrete: Microstructure, Properties and Materials. São Paulo: IBRACON, 2014.

MICHIE, C. **Optical Fiber Sensors for Advanced Composite Materials.** Comprehensive Composite Materials, Volume 5, 2000.

MULTON, S., CYR, M., SELLIER, A., DIEDERICH, P., PETIT, L. **Effects of aggregate size and alkali content on ASR expansion.** Cement and Concrete Research, 40(4), 2010.

MULTON, S. CYR, M., SELLIER, A., LEKLOU, A. &. PETIT, L. **Coupled effects of aggregate size and alkali content on ASR expansion.** Cement and Concrete Research, Elsevier, 38 (3), 2007.

MULTON, S., SEIGNOL, J. F., and TOUTLEMONDE, F., **Structural behavior of concrete beams affected by alkali-silica reaction.** ACI Materials Journal, 102(2), 2005.

NEVILLE, A. M. **Properties of Concrete**. **4th Edition**, Addision **Wesley Longman**, Edinburgh, 2004.

NIXON, P. J., SIMS, I. – **RILEM: State-of-the-Art Report of the RILEM Technical Committee** 219-ACS, 2016.

NOEL, M., SANCHEZ, L., TAWIL, D; **Structural Implications of Internal Swelling Reactions in Concrete: Review & Research Needs** Article in Magazine of Concrete Research, 2017.

PAN, J.W.; FENG, Y.T.; WANG, J.T.; SUN, Q.C.; ZHANG, C.H.; OWEN D.R.J **Modeling of alkali-silica reaction in concrete : a review**. Frontiers of Structural and Civil Engineering, v.6, n.1, p.1-18, 2012.

PAVOINE, A., DIVET, L., FENOUILLET, S., **A concrete performance test for delayed ettringite formation: Part I optimisation**. Cem. Concr. Res. 36, 2006.

PEI, H., LI, Z., ZHANG, B., MA, H., **Multipoint measurement of early age shrinkage in low w/c ratio mortars by using fiber Bragg gratings.** Mater. Lett. 131, 2014.

PETERSON, M. G., ULM, F.J. **Chemoplasticity of the alkali-silica reaction in concrete: modeling of stress-induced anisotropy**, report, departament of Civil & Enviromental engineering, Massachusetts, EUA, 2000.

PIGNATELLI, R. **Modelling of degradation induced by alkali-silica reaction in concrete structures**. Tese Politecnico di Milano, 2012.

POSTERLLI, M. C. **Expansion modeling due to the alkali-aggregate reaction of reinforced and fiber-reinforced concrete.** 2017. 168 f. Dissertation (Master in Civil Engineering) - São Carlos School of Engineering, University of São Paulo. 2017. (in portuguese)

RAMAKRISHNAN, M., RAJAN, G., SEMENOVA, Y., FARRELL, **G. Overview of Fiber Optic Sensor Technologies for Strain/Temperature Sensing Applications in Composite Materials.** Sensors, 16(1), 2016.

ROCHA R. P. O., JAREK A. , DIVINO P. L., DE MELO A. V., DE CARVALHO A. L., MEDEIROS B. L., DE LACERDA, L. A. **Installation of fiber optic sensors for AAR expansion monitoring in PETI DAM**. ICOLD-2013 International Symposium, Seattle, USA, 2013.

SABRI, N., ALJUNID, S. A., SALIM, M. S., & FOUAD, S. **Fiber Optic Sensors: Short Review and Applications**. Springer Series in Materials Science, 2014

SAHA, A.K.; KHAN, M.N.N.; SARKER, P.K.; SHAIKH, F.A.; PRAMANIK, A.; **The ASR mechanism of reactive aggregates in concrete and its mitigation by fly ash: A critical review.** Constr. Build. Mater. 171, 2018.

ŠAHINAGIĆ-ISOVIĆ, M. & MARKOVSKI, G. & CECEZ, M. **Shrinkage strain of concrete - Causes and types**. Građevinar. 64. 727-734. (2012).

SANCHEZ, L. F. M. **Contribution to the study of test methods in the evaluation of alkali aggregate reactions in concretes. Dissertation** (Master of Civil Engineering) - University of São Paulo. 2008 (in Portuguese)

SANCHEZ, L. F. M. KUPERMAN, S. C., HELENE, P. **Using the accelerated Brazilian concrete prism test (ABCPT) to evaluate alkali aggregate reaction (AAR)-**IBRACON, 2011.

SAKATA, K.; SHIMOMURA, T. **Recent progress in research on and evaluation of concrete creep and shrinkage in Japan**, Journal of Advanced Concrete Technology 2(2): 133–140, 2004.

SAOUMA, V.E.; MARTIN, R.A.; HARIRI-ARDEBILI, M. A.; KATAYAMA, T. A.; **Mathematicam model for the kinetics of the alkali-silica reaction.** Cement and Concrete Research, V68, 2015.

SCHERER, G. W. **Crystallisation in pores.** Cement and concrete research, 29(8), 1999.

SELLIER, A.; MULTON, S.; BUFFO-LACARRIÈRE, L.; VIDAL, T.; BOURBON, X; GUILLAUME, C. **Concrete creep modelling for structural applications: non-linearity, multiaxiality, hydration, temperature and drying effects**. Cement and Concrete Research, Elsevier, v. 79, p. 301-315, 2016.

SHAYAN, A. **Effects of alkali–aggregate reaction on concrete and structures.** Proceedings of the Institution of Civil Engineers - Construction Materials, 169(3), 2016.

SIMS, I., POOLE, A. B. **Alkali-Aggregate Reaction in Concrete: A World Review.** CRC Press, 2017

STANTON, T. E. **Expansion of concrete throught reaction between cement and aggregate.** Proceedings, ASCE, USA, 1940

SWAMY, R.N. and AL-ASALI, M.M. "**Engineering Properties of Concrete Affected by Alkali-Silica Reaction**." ACI Materials Journal Vol. 85 No. 5, 1988.

SWAMY, R.N. **The Alkali-Silica Reaction in Concrete.** Edited by R.N. Swamy, London, 1992.

TAHERI, S., **A review on five key sensors for monitoring of concrete structures.** Constr. Build. Mater. 204, 2019.

TAYLOR, H.F.W., FAMY, C., SCRIVENER, K.L**., Delayed ettringite formation.** Cement and Concrete Res. 31, 2001.

THOMAS M. D. A., FOLLIARD, K. J., FOURNIER, B., RIVARD, P., DRIMALAS, T., **Methods for Evaluating and Treating ASR-Affected Structures: Results of**

Field Application and Demonstration Projects – Volume I: Summary of Findings and Recommendations, Austin, 2013

THOMAS, M.D.A., FOURNIER, B., FOLLIARD, K.J. **Alkali-Aggregate Reactivity (AAR) Facts Book** Office of Pavement Technology Federal Highway Administration march 2013.

THOMAS, M; FOURNIER, B; FOLLIARD, K; IDEKER, J; E SHEHATA, M; **Test methods for Evaluating preventive measures for controling expansion due the álcali-silica reaction in concrete.** Paper. Cement and Concrete Research, 2006.

WIGUM, B.J., PEDERSEN, L.T., GRELK, B., LINDGARD, J. **State-of-the-art report: key parameters influencing the alkali aggregate reaction.** PARTNER project (report 2.1), SINTEF, 2006.

YU GE, MOHAMMED Z.E.B. ELSHAFIE, SAMIR DIRAR, CAMPBELL R.MIDDLETON. **The response of embedded strain sensors in concrete beams subjected to thermal loading,** Construction and Building Materials Volume 70, 15 November, 2014

YEHIA, S., LANDOLSI, T., HASSAN, M., & HALLAL, M. **Monitoring of strain induced by heat of hydration, cyclic and dynamic loads in concrete structures using fiber-optics sensors.** Measurement, 52, 2014.

YU, Z., JIAN, M., HU, S., and XIAODONG, S. **Delayed Ettringite Formation in Fly Ash Concrete under Moist Curing Conditions** 5th International Conference on Durability of Concrete Structures - Shenzhen University, Shenzhen, Guangdong Province, P.R.China July 2016

STANDARDS

AASTHO T 380-18 - Potential Alkali Reactivity of Aggregates and Effectiveness of ASR Mitigation Measures - miniature concrete prism test (MCPT)

ABNT NBR NM 45: 2006 Aggregates - Determination of the unit weight and air-void contents

ASTM C 157/C 157M, “Standard Test Method for Length Change of Hardened Hydraulic-Cement Mortar and Concrete,” Annual Book of ASTM Standards, Vol. 04.02 – Concrete and Aggregates, ASTM International, Conshohocken, PA, 2008.

ASTM C1293-18a, Standard Test Method for Determination of Length Change of Concrete Due to Alkali-Silica Reaction, ASTM International, West Conshohocken, PA, 2018

CSA A23.2-14 - Standard Test Method for Standard Test Method for Length Change of Concrete Due to Alkali-Carbonate Rock Length Change of Concrete Due to Alkali-Carbonate Rock Reaction Reaction

NF EN 197-1 - Cement - Part 1 : composition, specifications and conformity criteria for common cements, 2012

RILEM - Recommendations for the Prevention of Damage by Alkali-Aggregate Reactions in New Concrete Structures, 2016

NBR 15577-6:2018 - Aggregates - Alkali-aggregate reactivity Part 6: Determination of expansion on concrete prisms.)